# Gravitational waves from stochastic scalar fluctuations

Reza Ebadi,[1,2] Soubhik Kumar,[3,4] Amara McCune,[3,4,5] Hanwen Tai,[6] and Lian-Tao Wang[6,7,8]

[1]*Department of Physics, University of Maryland, College Park, Maryland 20742, USA*
[2]*Quantum Technology Center, University of Maryland, College Park, Maryland 20742, USA*
[3]*Berkeley Center for Theoretical Physics, Department of Physics, University of California, Berkeley, California 94720, USA*
[4]*Theoretical Physics Group, Lawrence Berkeley National Laboratory, Berkeley, California 94720, USA*
[5]*Department of Physics, University of California, Santa Barbara, California 93106, USA*
[6]*Department of Physics, The University of Chicago, Chicago, Illinois 60637, USA*
[7]*Enrico Fermi Institute, University of Chicago, Chicago, Illinois 60637, USA*
[8]*Kavli Institute for Cosmological Physics, University of Chicago, Chicago, Illinois 60637, USA*

(Received 4 October 2023; accepted 15 March 2024; published 15 April 2024)

We present a novel mechanism for gravitational wave generation in the early Universe. Light spectator scalar fields during inflation can acquire a blue-tilted power spectrum due to stochastic effects. We show that this effect can lead to large curvature perturbations at small scales (induced by the spectator field fluctuations) while maintaining the observed, slightly red-tilted curvature perturbations at large cosmological scales (induced by the inflaton fluctuations). Along with other observational signatures, such as enhanced dark matter substructure, large curvature perturbations can induce a stochastic gravitational wave background (SGWB). The predicted strength of SGWB in our scenario, $\Omega_{\rm GW}h^2 \simeq 10^{-20}$–$10^{-15}$, can be observed with future detectors, operating between $10^{-5}$ Hz and 10 Hz. We note that, in order to accommodate the newly reported NANOGrav observation, one could consider the same class of spectator models. At the same time, one would need to go beyond the simple benchmark considered here and consider a regime in which a misalignment contribution is also important.

DOI: 10.1103/PhysRevD.109.083519

## I. INTRODUCTION

The fluctuations observed in the cosmic microwave background (CMB) and large-scale structure (LSS) have given us valuable information about the primordial Universe. As per the standard ΛCDM cosmology, such fluctuations were generated during a period of cosmic inflation (see [1] for a review). While the microphysical nature of inflation is still unknown, well-motivated single-field slow-roll inflationary models predict an approximately scale-invariant spectrum of primordial fluctuations, consistent with CMB and LSS observations. These observations have enabled precise measurements of the primordial fluctuations between the comoving scales $k \sim 10^{-4} - 1\ \mathrm{Mpc}^{-1}$. However, the properties of primordial density perturbations are comparatively much less constrained for $k \gtrsim \mathrm{Mpc}^{-1}$. In particular, as we will discuss below, the primordial curvature power spectrum $\Delta_\zeta^2$ can naturally be much larger at such small scales, compared to the value $\Delta_\zeta^2 \approx 2 \times 10^{-9}$ observed on CMB scales [2].

Scales corresponding to $k \gtrsim \mathrm{Mpc}^{-1}$ are interesting for several reasons. First, they contain vital information regarding the inflationary dynamics after the CMB-observable modes exit the horizon. In particular, they can reveal important clues as to how inflation could have ended and the Universe was reheated. An enhanced power spectrum on such scales can also lead to overabundant dark matter (DM) subhalos, motivating novel probes (see [3] for a review). Furthermore, if the enhancement is significant, $\Delta_\zeta^2 \gtrsim 10^{-7}$, the primordial curvature fluctuations can induce a stochastic gravitational wave background (SGWB) within the range of future gravitational wave detectors [4]. For even larger fluctuations, $\Delta_\zeta^2 \gtrsim 10^{-2}$, primordial black holes (PBH) can form, leading to interesting observational signatures [5,6]. Given this, it is interesting to look for mechanisms that can naturally lead to a "blue-tilted," enhanced power spectrum at small scales.

In models involving a single dynamical field during inflation, such an enhancement can come, for example, from an inflection point on the inflaton potential or an ultraslow roll phase [7–11].[1] However, for any generic structure of the inflaton potential, a power spectrum that is blue-tilted at small scales can naturally arise if there are additional light scalar fields other than the inflaton field. One class of such mechanisms involves a rolling complex scalar field where the radial mode $\varphi$ has a mass of order the

[1]See also [12] for PBH formation in a multifield ultraslow roll inflationary model.

 

inflationary Hubble scale $H$ and is initially displaced away from the minimum [13]. As $\varphi$ rolls down the inflationary potential, the fluctuations of the Goldstone mode $\propto (H/\varphi)^2$ increase with time. This can then give rise to *isocurvature* fluctuations that increase with $k$, i.e., a blue-tilted spectrum. This idea was further discussed in [14] to show how *curvature* perturbations can be enhanced on small scales as well, and lead to the formation of PBH. For further studies on blue-tilted isocurvature perturbations, see, e.g., [15–18]. Other than this, models of vector DM [19], early matter domination [20], and incomplete phase transitions [21] can also give rise to enhanced curvature perturbation at small scales.

In this work, we focus on a different mechanism where a Hubble-mass scalar field quantum mechanically fluctuates around the minimum of its potential, instead of being significantly displaced away from it (as in [13,14]).[2] Hubble-mass fields can naturally roll down to their minimum since the homogeneous field value decreases with time as $\exp(-m^2 t/(3H))$, where $m$ is the mass of the field with $m \lesssim H$. Given that we do not know the *total* number of $e$-foldings that took place during inflation, it is plausible that a Hubble mass particle was already classically driven to the minimum of the potential when the CMB-observable modes exit the horizon during inflation. For example, for $m^2/H^2 = 0.2$, the field value decreases by approximately a factor of $10^3$, for $100e$-foldings of inflation prior to the exit of the CMB-observable modes. For any initial field value $\varphi_{\rm ini} \lesssim 10^3 \langle\varphi\rangle$, this can then naturally localize the massive field near the minimum $\langle\varphi\rangle$. However, the field can still have quantum mechanical fluctuations which tend to diffuse the field away from $\langle\varphi\rangle$. The potential for the field, on the other hand, tries to push the field back to $\langle\varphi\rangle$. The combination of these two effects gives rise to a nontrivial probability distribution for the field, both as a function of time and space.

We study these effects using the stochastic formalism [23,24] for light scalar fields in de Sitter (dS) spacetime. In particular, such stochastic effects can lead to a spectrum that is blue-tilted at small scales. While we carry out the computation by solving the associated Fokker-Planck equation in detail below, we can intuitively understand the origin of a blue-tilted spectrum as follows. For simplicity, we momentarily restrict our discussion to a free scalar field $\sigma$ with mass $m$ such that $m^2 \lesssim H^2$. The fluctuation $\sigma_k(t)$, corresponding to a comoving $k$-mode, decays after horizon exit as $\sigma_k(t) \sim H \exp(-m^2(t - t_*)/(3H))$, where $t_*$ is the time when the mode exits the horizon, $k = a(t_*)H$. We can rewrite the above by noting that physical momenta redshift as a function of time via $k/a(t) = H \exp(-H(t - t_*))$.

[2]For scenarios where the spectator field fluctuates around the minimum and gives rise to dark matter abundance, see, e.g., [22].

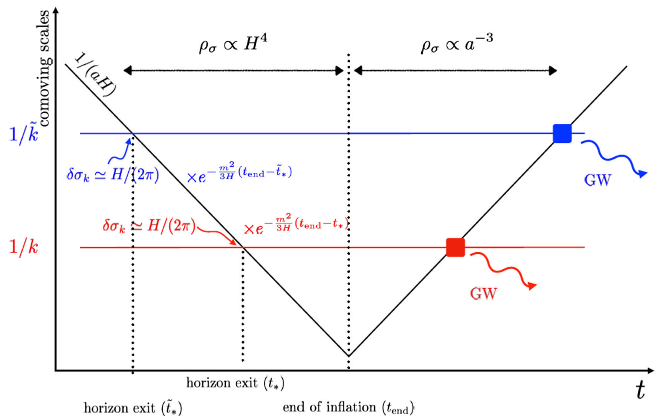


FIG. 1. Schematic of the mechanism. The comoving horizon $1/(aH)$ decreases during inflation and increases after that. Any $k$-mode carries a fluctuation of order $H/(2\pi)$ at the time of mode exit. However, modes with larger $k$ (red) exit the horizon later and encounters less dilution compared to modes with smaller $k$ (blue), since $t_* > \tilde{t}_*$. Consequently, modes with larger $k$ source stronger gravitational waves upon horizon reentry (shown via square box). We also depict the fact that $\sigma$ carries an energy density $\propto H^4$ during inflation, and dilutes as matter (for our benchmark choices) after inflation ends.

Then we arrive at, $\sigma_k(t) \sim H(k/(aH))^{m^2/(3H^2)}$. Therefore, the dimensionless power spectrum, $|\sigma_k|^2 k^3 \propto (k/(aH))^{2m^2/(3H^2)}$ has a blue tilt of $2m^2/(3H^2)$. Physically, modes with smaller values of $k$ exit the horizon earlier and get more diluted compared to modes with larger values of $k$, leading to more power at larger $k$, and thus a blue-tilted spectrum. This qualitative feature, including the specific value of the tilt for a free field, is reproduced by the calculation described later where we also include the effects of a quartic self-coupling. We summarize the mechanism in Fig. 1.

We note that if $m$ is significantly smaller than $H$, the tilt is reduced and the observational signatures are less striking. On the other hand, for $m \gtrsim H$, the field is exponentially damped, and stochastic effects are not efficient in displacing the field away from the minimum. Therefore, it is puzzling as to why the particle mass, *a priori* arbitrary, could be close to $H$ in realistic scenarios. However, a situation with $m \approx H$ can naturally rise if the field is nonminimally coupled to gravity. That is, a coupling $\mathcal{L} \supset cR\sigma^2$, where $R$ is the Ricci scalar, can uplift the particle mass during inflation $m^2 = (c/12)H^2$, regardless of a smaller "bare" mass. Here we have used $R = (1/12)H^2$ during inflation, and we notice for $c \sim \mathcal{O}(1)$, we can have a non-negligible blue-tilted spectrum.

The way the spectrum of $\sigma$ affects the curvature perturbation depends on the cosmology, and in particular, the lifetime of $\sigma$. During inflation, the energy density stored in $\sigma$ is of order $H^4$, as expected, since $\sigma$ receives $H$-scale quantum fluctuations. This is subdominant compared to the energy stored in the inflaton field $\sim H^2 M_{\rm pl}^2$. This implies $\sigma$

acts as a spectator field during inflation, and through the stochastic effects, $\sigma$ obtains isocurvature fluctuations. After the end of inflation, $\sigma$ dilutes as matter while the inflaton decay products dilute as radiation. Therefore, similar to the curvaton paradigm [25–28], the fractional energy density in $\sigma$ increases with time. Eventually, $\sigma$ decays into Standard Model radiation, and its isocurvature perturbations get imprinted onto the curvature perturbation. Different from the curvaton paradigm, in our scenario, $\sigma$ does not dominate the energy density of the Universe, and also the fluctuations of the inflaton are not negligible. In particular, on large scales, observed via CMB and LSS, the fluctuations are red-tilted and sourced by the inflaton, as in ΛCDM cosmology. On the other hand, the blue-tilted $\sigma$ fluctuations are subdominant on those scales, while dominant at smaller scales $\lesssim$Mpc. These enhanced perturbations can source an SGWB, observable in future gravitational wave detectors, as we describe below.

The rest of the work is organized as follows. In Sec. II, we describe the evolution of the inflaton field and $\sigma$ along with some general properties of curvature perturbation in our framework. In Sec. III, we compute the stochastic contributions to $\sigma$ fluctuations to obtain its power spectrum. We then use these results in Sec. IV to determine the full shape of the curvature power spectrum, both on large and small scales. The small-scale enhancement of the curvature power spectrum leads to an observable SGWB and we evaluate the detection prospects in Sec. V in the context of $\mu$-Hz to Hz-scale gravitational wave detectors. We conclude in Sec. VI. We include some technical details relevant to the computation of SGWB in Appendix A.

## II. COSMOLOGICAL HISTORY AND CURVATURE PERTURBATION

We now describe in detail the cosmological evolution considered in this work. We assume that the inflaton field $\phi$ drives the expansion of the Universe during inflation and the quantum fluctuations of $\phi$ generate the density fluctuations that we observe in the CMB and LSS, as in standard cosmology. We also assume that there is a second real scalar field $\sigma$ which behaves as a subdominant spectator field during inflation, as alluded to above. We parametrize its potential as,

$$V(\sigma) = \frac{1}{2}m^2\sigma^2 + \frac{1}{4}\lambda\sigma^4. \quad (1)$$

The $\sigma$ field does not drive inflation but nonetheless obtains quantum fluctuations during inflation. In particular, $\sigma$ obtains stochastic fluctuations around the minimum of its potential, as we compute in Sec. III. After the end of inflation, the inflaton is assumed to reheat into radiation with energy density $\rho_r$, which dominates the expansion of the Universe.

We have ignored the interaction between $\phi$ and $\sigma$. First, the two fields could be part of completely different sectors with no mediators that can couple the two sectors. Second, the inflaton can be modeled as a (pseudo)-Goldstone boson so that there is an approximate shift symmetry $\phi \to \phi +$ constant. This shift symmetry is necessary to explain the lightness of the inflaton field. Furthermore, this approximate shift symmetry leads to an almost scale-invariant power spectra on large scales, observed in the CMB. In the presence of this symmetry, the leading operator that couples the two fields is of the type $(\partial\phi)^2\sigma^2/\Lambda^2$ with some effective theory cutoff scale $\Lambda$. Here we are assuming a $\sigma \to -\sigma$ symmetry which is present in the potential $V(\sigma)$ (1). The cutoff scale can be high, for example, of the order of the Planck scale. This interaction can then be safely ignored.

The evolution of the $\sigma$ field depends on its mass $m$, interaction $\lambda$, and its frozen (root mean squared) displacement $\sigma_0$ during inflation. As long as the "effective" mass of $\sigma$: $m^2 + 3\lambda\sigma_0^2$, is smaller than the Hubble scale, $\sigma$ remains approximately frozen at $\sigma_0$. However, after the Hubble scale falls below the effective mass, $\sigma$ starts oscillating around its potential. The evolution of its energy density $\rho_\sigma$, during this oscillatory phase depends on the values of $m$ and $\lambda$. If the quartic interactions dominate, with $\lambda\sigma^2 \gg m^2$, $\rho_\sigma$ dilutes like radiation [29]. Eventually, the amplitude of $\sigma$ decreases sufficiently, so that $\lambda\sigma^2 \lesssim m^2$, following which $\rho_\sigma$ starts redshifting like matter. We illustrate these behaviors in Fig. 2.

Similar to the curvaton paradigm [25–28], during the epoch $\rho_\sigma$ is diluting as matter, its fractional energy density,

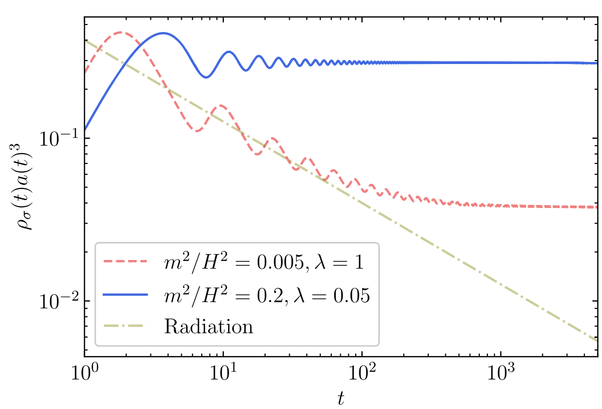


FIG. 2. Time evolution of scalar field energy density $\rho_\sigma(t)$. In scenarios where the quartic term dominates the initial evolution (dashed red), the field dilutes as radiation (dot-dashed olive), $\rho_\sigma(t) \propto 1/a(t)^4$. Eventually, the mass term becomes important, and the behavior becomes $\rho_\sigma(t) \propto 1/a(t)^3$. The benchmark choices in this work will mimic the blue curve where the evolution of $\rho_\sigma(t)$ is always dominated by the mass term with a matter-like dilution. For both the blue and the red curves, $t = 1$ corresponds to the moment when the Hubble scale is approximately equal to the effective mass and the field starts oscillating.

$f_\sigma(t) \equiv \rho_\sigma(t)/\rho_r(t)$, increases linearly with the scale factor $a(t)$. For our benchmark parameter choices, we assume $\sigma$ to decay into SM radiation while $f_\sigma(t_d) \sim 1$, where $t_d$ denotes the time of $\sigma$ decay. After $t_d$, the evolution of the Universe coincides with standard cosmology.

With this cosmology in mind, we can track the evolution of various cosmological perturbations using the gauge invariant quantity $\zeta$, the curvature perturbation on uniform-density hypersufaces [30],

$$\zeta = -\psi - H\frac{\delta\rho}{\dot{\rho}}. \tag{2}$$

Here $\psi$ is a fluctuation appearing in the spatial part of the metric as, $\delta g_{ij} = -2a^2\psi\delta_{ij}$ (ignoring vector and tensor perturbations), $\delta\rho$ denotes a fluctuation around a homogeneous density $\rho$, and an overdot denotes a derivative with respect to physical time $t$. We assume that the decay products of $\phi$ do not interact with $\sigma$ during their cosmological evolution. Since there is no energy transfer between the two sectors, their energy densities evolve as,

$$\dot{\rho}_r = -4H\rho_r, \qquad \dot{\rho}_\sigma = -3H\rho_\sigma, \tag{3}$$

where we have focused on the epoch where $\sigma$ dilutes like matter. For the benchmark parameter choices discussed below, the matterlike dilution for $\sigma$ onsets soon after inflation. Similar to Eq. (2), we can parametrize gauge invariant fluctuations in radiation and $\sigma$ with the variables,

$$\zeta_r = -\psi + \frac{1}{4}\frac{\delta\rho_r}{\rho_r}, \qquad \zeta_\sigma = -\psi + \frac{1}{3}\frac{\delta\rho_\sigma}{\rho_\sigma}. \tag{4}$$

In terms of the above variables, we can express Eq. (2) as,

$$\zeta = \frac{4}{4+3f_\sigma}\zeta_r + \frac{3f_\sigma}{4+3f_\sigma}\zeta_\sigma = \zeta_r + \frac{f_\sigma}{4+3f_\sigma}S_\sigma. \tag{5}$$

Here $S_\sigma \equiv 3(\zeta_\sigma - \zeta_r)$ is the isocurvature perturbation between radiation and $\sigma$ perturbations. In the absence of any energy transfer, $\zeta_r$ and $\zeta_\sigma$ are each conserved at superhorizon scales [31]. As a result, the evolution of $\zeta$ is entirely determined by the time-dependent relative energy density of between radiation and $\sigma$, $f_\sigma = \rho_\sigma/\rho_r$. Since $\zeta_r$ and $S_\sigma$ are uncorrelated, the power spectrum for curvature perturbation $\langle\zeta(\mathbf{k})\zeta(\mathbf{k}')\rangle \equiv (2\pi)^3\delta(\mathbf{k}+\mathbf{k}')P_\zeta(k)$ is determined by,

$$P_\zeta(k) = P_{\zeta_r}(k) + \left(\frac{f_\sigma}{4+3f_\sigma}\right)^2 P_{S_\sigma}(k), \tag{6}$$

or equivalently,

$$\Delta^2_\zeta(k) = \Delta^2_{\zeta_r}(k) + \left(\frac{f_\sigma}{4+3f_\sigma}\right)^2 \Delta^2_{S_\sigma}(k), \tag{7}$$

where $\Delta^2_\zeta(k) = k^3P_\zeta(k)/(2\pi^2)$, with $\Delta^2_{\zeta_r}(k)$ and $\Delta^2_{S_\sigma}(k)$ defined analogously.

To compute the spectral tilt, we denote the comoving momentum of the mode that enters the horizon at $t_d$, the time of $\sigma$ decay, as $k_d$ which satisfies $k_d = a(t_d)H(t_d)$. For $t > t_d$, $\zeta$ remains conserved with time on superhorizon scales. Correspondingly, for $k < k_d$, the spectral tilt is given by,

$$n_s - 1 \equiv \frac{\mathrm{d}\ln\Delta^2_\zeta(k)}{\mathrm{d}\ln k} = \frac{\Delta^2_{\zeta_r}(k)}{\Delta^2_\zeta(k)}\frac{\mathrm{d}\ln\Delta^2_{\zeta_r}(k)}{\mathrm{d}\ln k} + \left(\frac{f_\sigma}{4+3f_\sigma}\right)^2\frac{\Delta^2_{S_\sigma}(k)}{\Delta^2_\zeta(k)}\frac{\mathrm{d}\ln\Delta^2_{S_\sigma}(k)}{\mathrm{d}\ln k}. \tag{8}$$

We will consider scenarios where the radiation energy density $\rho_r$ originates from the inflaton, and therefore, $\mathrm{d}\ln\Delta^2_{\zeta_r}(k)/\mathrm{d}\ln k \approx -0.04$ determines the spectral tilt observed on CMB scales [2]. On the other hand, $\sigma$ acquires stochastic fluctuations to give rise to a blue-tilted power spectrum with $\mathrm{d}\ln\Delta^2_{S_\sigma}(k)/\mathrm{d}\ln k \sim 0.3$, as discussed next in Sec. III. Since we will be interested in scenarios with $f_\sigma \lesssim 1$, i.e., $(f_\sigma/(4+3f_\sigma))^2 \lesssim 0.02$, we require $\Delta^2_{S_\sigma}(k)/\Delta^2_\zeta(k) \lesssim 1$ on CMB-scales to be compatible with CMB measurements of $n_s$. We can also compute the running of the tilt,

$$\frac{\mathrm{d}n_s}{\mathrm{d}\ln k} \approx \left(\frac{f_\sigma}{4+3f_\sigma}\right)^2\frac{\Delta^2_{S_\sigma}(k)}{\Delta^2_\zeta(k)}\frac{(\mathrm{d}\ln\Delta^2_{S_\sigma}(k)^2}{\mathrm{d}\ln k)}. \tag{9}$$

Our benchmark parameter choices, discussed above, thus also satisfy the CMB constraints on $\mathrm{d}n_s/\mathrm{d}\ln k$ [2].

## III. REVIEW OF THE STOCHASTIC FORMALISM

A perturbative treatment of self-interacting light scalar fields in de Sitter (dS) spacetime is subtle due to infrared divergences. A stochastic approach [23,24] can be used to capture the nontrivial behavior of such fields in dS. In this formalism, the superhorizon components of the fields are considered classical stochastic fields that satisfy a Langevin equation, which includes a random noise originating from the subhorizon physics. This gives rise to a Fokker-Planck equation for the probability distribution function (PDF) of the stochastic field, which can be used to calculate correlation functions of physical observables. We now review these ideas briefly while referring the reader to refs. [23,24,32–35] for more details.

### A. Langevin and Fokker-Planck equations

The stochastic approach provides an effective description for the long-wavelength, superhorizon sector of the field theory by decomposing the fields into long-wavelength classical components and short-wavelength quantum operators. For instance, a light scalar field can be decomposed as

$$\sigma_{\rm tot}(\mathbf{x},t) = \sigma(\mathbf{x},t) + \int \frac{{\rm d}^3k}{(2\pi)^3}\theta(k-\epsilon a(t)H)e^{-i\mathbf{k}\cdot\mathbf{x}}(a_{\mathbf{k}}u_k + a^\dagger_{-\mathbf{k}}u_k^*), \tag{10}$$

where $\theta(\cdots)$ is the Heaviside step function, $a$ is the scale factor, $H$ is the Hubble scale, and $\epsilon \lesssim 1$ is a constant number (not to be confused with the slow-roll parameter) which defines the boundary between long ($k < \epsilon a(t)H$) and short ($k > \epsilon a(t)H$) modes. We have also denoted the classical part of the field as $\sigma(\mathbf{x},t)$. The quantum description of the short modes is characterized by the creation and annihilation operators $a_{\mathbf{k}}, a^\dagger_{\mathbf{k}}$ along with the mode functions $u_k(t), u_k^*(t)$.

For a light field with $|V''(\sigma)| \ll H^2$, it can be shown [23,24,32,33] that the classical part of the field, $\sigma(\mathbf{x},t)$, follows a Langevin equation

$$\dot\sigma(\mathbf{x},t) = -\frac{1}{3H}V'(\sigma) + \xi(\mathbf{x},t). \tag{11}$$

Here an overdot and a prime denote derivative with respect to time and the field, respectively. The noise $\xi$ arises from short-scale modes,

$$\xi(\mathbf{x},t) = \epsilon a H^2 \int \frac{{\rm d}^3k}{(2\pi)^3}\delta(k-\epsilon aH)e^{-i\mathbf{k}\cdot\mathbf{x}}(a_{\mathbf{k}}u_k + a^\dagger_{-\mathbf{k}}u_k^*), \tag{12}$$

with a correlation

$$\langle\xi(\mathbf{x}_1,t_1)\xi(\mathbf{x}_2,t_2)\rangle = \frac{H^3}{4\pi^2}\delta(t_1-t_2)j_0(\epsilon aH|\mathbf{x}_1-\mathbf{x}_2|), \tag{13}$$

where $j_0(x) = \sin x/x$ is the zeroth order spherical Bessel function. We see that the noise is uncorrelated in time (i.e., it is a white noise), but also it is uncorrelated over spatial separations larger than $(\epsilon aH)^{-1}$.

The Langevin equation (11) gives rise to a Fokker-Planck equation for the one-point PDF,

$$\frac{\partial P_{\rm FP}(t,\sigma(\mathbf{x},t))}{\partial t} = \left[\frac{V''(\sigma(\mathbf{x},t))}{3H} + \frac{V'(\sigma(\mathbf{x},t))}{3H}\frac{\partial}{\partial\sigma} + \frac{H^3}{8\pi^2}\frac{\partial^2}{\partial\sigma^2}\right]P_{\rm FP}(t,\sigma(\mathbf{x},t)). \tag{14}$$

Here $P_{\rm FP}(t,\sigma(\mathbf{x},t))$ is the PDF of the classical component to take the value $\sigma(\mathbf{x},t)$ at time $t$. Thus the Fokker-Planck equation describes how an ensemble of field configurations evolves as a function of time, according to the underlying Langevin equation. In this equation, the first and second terms on the right-hand side represent classical drift terms that depend on the potential $V(\sigma)$. The third term represents a diffusion contribution from the noise $\xi$. While the classical drift tries to move the central value of the field toward the minimum of the potential, the diffusion contribution pushes the field away from the minimum. An equilibrium is achieved when these two effects balance each other. This equilibrium solution can be obtained by setting $\partial P_{\rm FP}/\partial t = 0$ in (14), and is given by

$$P_{\rm FP,eq}(\sigma) = \frac{1}{\mathcal{N}}\exp\left(-\frac{8\pi^2}{3H^4}V(\sigma)\right), \tag{15}$$

where $\mathcal{N}$ is a normalization constant. Upon a variable change

$$\tilde P_{\rm FP}(t,\sigma) \equiv \exp\left(\frac{4\pi^2V(\sigma)}{3H^4}\right)P_{\rm FP}(t,\sigma), \tag{16}$$

eq. (14) can written as

$$\frac{\partial\tilde P_{\rm FP}(t,\sigma)}{\partial t} = \frac{H^3}{4\pi^2}\underbrace{\left[-\frac{1}{2}(v'^2-v'') + \frac{1}{2}\frac{\partial^2}{\partial\sigma^2}\right]}_{D_\sigma}\tilde P_{\rm FP}(t,\sigma), \tag{17}$$

with $v(\sigma) = 4\pi^2V(\sigma)/(3H^4)$. We can recast the above as an eigenvalue equation. To that end, we write

$$\tilde P_{\rm FP}(t,\sigma) = \sum_n a_n e^{-\Lambda_n t}\psi_n(\sigma), \tag{18}$$

where $\psi_n(\sigma)$ satisfies the equation

$$D_\sigma\psi_n(\sigma) = -\frac{4\pi^2}{H^3}\Lambda_n\psi_n(\sigma). \tag{19}$$

The eigenfunctions $\psi_n(\sigma)$ form an orthonormal basis of functions and $a_n$'s are some arbitrary coefficients.

This time-independent eigenvalue equation (19) can be solved numerically for a generic potential $V(\sigma)$, as we discuss below with an example. By definition, and independent of the form of the potential, the eigenfunction $\psi_0$ corresponding to the eigenvalue $\Lambda_0 = 0$, determines the equilibrium distribution. Solution of the Eq. (19) for $\Lambda_0 = 0$ is given by

$$\psi_0(\sigma) = \frac{1}{\sqrt{\mathcal{N}}}\exp\left(-\frac{4\pi^2}{3H^4}V(\sigma)\right). \tag{20}$$

Thus comparing to Eq. (15) we get,

$$P_{\rm FP,eq}(\sigma) = \psi_0(\sigma)^2. \tag{21}$$

### B. Two-point correlation function and power spectrum

We are interested in calculating the two-point correlation functions of cosmological perturbations. Any such two-point correlation function depends only on the geodesic distance $s$ between the two points. Given the coordinates of the two points $(\mathbf{x}_1, t_1)$ and $(\mathbf{x}_2, t_2)$, this distance can be parametrized by $z = 1 + H^2 s^2/2$ with

$$z = \cosh H(t_1 - t_2) - \frac{1}{2} e^{H(t_1+t_2)} (H|\mathbf{x}_1 - \mathbf{x}_2|)^2. \tag{22}$$

To understand the significance of the variable $z$, we first write the two-point correlation function for an arbitrary function of $\sigma$, $g(\sigma)$, as

$$G_g(\mathbf{x}_1, t_1; \mathbf{x}_2, t_2) = \langle g(\sigma(\mathbf{x}_1, t_1)) g(\sigma(\mathbf{x}_2, t_2)) \rangle. \tag{23}$$

To compute this, it is more convenient to calculate the temporal correlation first, and then use the fact that equal-time correlations over spatially separated points are related to the temporal correlation through the de Sitter-invariant variable $z$ (22). In particular, for coincident points $G_g$ is a function of $(t_1 - t_2)$ only, which can be expressed in terms of $z$ for large $|z|$ as,

$$G_g(t_1 - t_2) \approx G_g(H^{-1} \ln|2z|). \tag{24}$$

However, for an equal time correlation function we can also write,

$$|2z| \approx (He^{Ht}|\mathbf{x}_1 - \mathbf{x}_2|)^2, \tag{25}$$

which gives,

$$G_g(t_1 - t_2) \simeq G_g\left(\frac{\ln|2z|}{H}\right) \simeq G_g\left(\frac{2}{H}\ln(aH|\mathbf{x}_1 - \mathbf{x}_2|)\right), \tag{26}$$

where the approximations hold as long as $|z| \gg 1$ and we used $a(t) = \exp(Ht)$.

Now we aim at formally calculating $G_g(t)$ in terms of solutions of the Fokker-Planck equation. The temporal correlation can be written as (see, e.g., [23,24,35])

$$G_g(t) = \int \mathrm{d}\sigma \int \mathrm{d}\sigma_0 P_{\mathrm{FP,eq}}(\sigma_0) g(\sigma_0) \Pi(t, \sigma; \sigma_0) g(\sigma), \tag{27}$$

where $\Pi(t, \sigma; \sigma_0)$ is the kernel function of the time evolution of the probability distribution function, i.e., if the probability distribution is $\delta(\sigma - \sigma_0)$ at $t = 0$ it would be $\Pi(t, \sigma; \sigma_0)$ at time $t$. In particular, it is defined by

$$P_{\mathrm{FP}}(t; \sigma) = \int \mathrm{d}\sigma_0 \Pi(t, \sigma; \sigma_0) P(0; \sigma_0). \tag{28}$$

In terms of rescaled probabilities, we can rewrite the above as,

$$\tilde{P}_{\mathrm{FP}}(t; \sigma) = \int \mathrm{d}\sigma_0 \tilde{\Pi}(t, \sigma; \sigma_0) \tilde{P}_{\mathrm{FP}}(0; \sigma_0), \tag{29}$$

$$\Pi(t, \sigma; \sigma_0) = e^{-v(\sigma)} \tilde{\Pi}(t, \sigma; \sigma_0) e^{v(\sigma_0)}. \tag{30}$$

It follows that $\tilde{\Pi}$ satisfies the same Fokker-Planck equation as $\tilde{P}_{\mathrm{FP}}$ (17). Therefore, the solutions can be written as

$$\tilde{\Pi}(t; \sigma, \sigma_0) = \sum_n \psi_n(\sigma_0) e^{-\Lambda_n t} \psi_n(\sigma), \tag{31}$$

which obeys the initial condition $\tilde{\Pi}(0; \sigma, \sigma_0) = \delta(\sigma - \sigma_0)$ is satisfied. Therefore, according to (27) we have[3]

$$G_g(t) = \sum_n \int \mathrm{d}\sigma_0 \psi_0(\sigma_0) g(\sigma_0) \psi_n(\sigma_0) e^{-\Lambda_n t} \times \int \mathrm{d}\sigma \psi_n(\sigma) g(\sigma) \psi_0(\sigma) = \sum_n g_n^2 e^{-\Lambda_n t}, \tag{32}$$

where

$$g_n \equiv \int \mathrm{d}\sigma \psi_n(\sigma) g(\sigma) \psi_0(\sigma). \tag{33}$$

We see that in late times the correlation is dominated by the smallest $\Lambda_n \neq 0$.

We can now present the equal-time correlation function by combining (26) and (32) [23,24,35]:

$$G_g(|\mathbf{x}_1 - \mathbf{x}_2|) = \sum_n \frac{g_n^2}{(aH|\mathbf{x}_1 - \mathbf{x}_2|)^{2\Lambda_n/H}}. \tag{34}$$

We note that this depends on the physical distance between the two points at time $t$, namely, $a|\mathbf{x}_1 - \mathbf{x}_2|$. This correlation function has the following dimensionless power spectrum [35],

$$\Delta_g^2(k) = \frac{k^3}{2\pi^2} P_g(k) = \frac{k^3}{2\pi^2} \int \mathrm{d}^3 r e^{-i\mathbf{k}\cdot\mathbf{r}} G_g(r) = \sum_n \frac{2g_n^2}{\pi} \Gamma\left(2 - \frac{2\Lambda_n}{H}\right) \sin\left(\frac{\pi\Lambda_n}{H}\right) \left(\frac{k}{aH}\right)^{2\Lambda_n/H} \tag{35}$$

where $\Gamma$ denotes the gamma function. This expression is valid in the limit $k \ll aH$. So far our discussion has been general and is valid for any potential under the slow-roll approximation and the assumption of a small effective

[3]Note that $P_{\mathrm{FP,eq}}(\sigma_0) = \psi_0(\sigma_0)^2 = \psi_0(\sigma_0)\psi_0(\sigma) e^{4\pi^2 V(\sigma)/3H^4} \times e^{-4\pi^2 V(\sigma_0)/3H^4}$.

mass, $|V''(\sigma)| \ll H^2$. In the next section, we discuss a concrete example with $V(\sigma)$ given in Eq. (1).

## IV. LARGE CURVATURE PERTURBATION FROM STOCHASTIC FLUCTUATIONS

We focus on the potential in Eq. (1) to demonstrate how large curvature perturbation can arise from stochastic fluctuations. We first describe various equilibrium quantities and how to obtain the power spectra $P_{S_\sigma}$, and consequently evaluate $P_\zeta$ which determines the strength of the GW signal.

### A. Equilibrium configuration

The normalized PDF for the one-point function is given by Eq. (15). For convenience, we reproduce it here

$$P_{\mathrm{FP,eq}}(\sigma) = \frac{1}{\mathcal{N}} \exp\left(-\frac{8\pi^2 V(\sigma)}{3H^4}\right), \tag{36}$$

with

$$\mathcal{N} = \frac{2\sqrt{2}\sqrt{\lambda}}{\exp\left(\frac{m^4\pi^2}{3H^4\lambda}\right) m K_{\frac{1}{4}}\left(\frac{m^4\pi^2}{3H^4\lambda}\right)}. \tag{37}$$

Here $K_n(x)$ is the modified Bessel function of the second kind. The mean displacement of the field can be computed as,

$$\langle\sigma^2\rangle = \int_0^\infty \mathrm{d}\sigma\sigma^2 P_{\mathrm{FP,eq}}(\sigma) = \frac{m^2}{2\lambda}\left(-1 + \frac{K_{\frac{3}{4}}\left(\frac{m^4\pi^2}{3H^4\lambda}\right)}{K_{\frac{1}{4}}\left(\frac{m^4\pi^2}{3H^4\lambda}\right)}\right). \tag{38}$$

In the appropriate limits, this can be simplified to,

$$\langle\sigma^2\rangle|_{\lambda\to 0} = \frac{3H^4}{8\pi^2 m^2}, \tag{39}$$

$$\langle\sigma^2\rangle|_{m\to 0} = \sqrt{\frac{3}{2\lambda}}\frac{\Gamma(3/4)}{\Gamma(1/4)\pi} H^2, \tag{40}$$

matching the standard results [24]. We can also compute the average energy density of the field as,

$$\begin{aligned}\langle V(\sigma)\rangle &= \int_0^\infty \mathrm{d}\sigma V(\sigma) P_{\mathrm{FP,eq}}(\sigma)\\ &= \frac{1}{32}\left(\frac{3H^4}{\pi^2} - \frac{4m^4}{\lambda} + \frac{4m^4}{\lambda}\frac{K_{\frac{3}{4}}\left(\frac{m^4\pi^2}{3H^4\lambda}\right)}{K_{\frac{1}{4}}\left(\frac{m^4\pi^2}{3H^4\lambda}\right)}\right),\end{aligned} \tag{41}$$

reducing to,

$$\langle V(\sigma)\rangle|_{\lambda\to 0} = \frac{3H^4}{16\pi^2}, \tag{42}$$

$$\langle V(\sigma)\rangle|_{m\to 0} = \frac{3H^4}{32\pi^2}. \tag{43}$$

To ensure that $\sigma$ does not dominate energy density during inflation, we require

$$\langle V(\sigma)\rangle \ll 3H^2 M_{\mathrm{pl}}^2. \tag{44}$$

Finally, we compute $\langle V''(\sigma)\rangle$ to check the validity of slow-roll of the $\sigma$ field,

$$\begin{aligned}\langle V''(\sigma)\rangle &= \int_0^\infty \mathrm{d}\sigma V''(\sigma) P_{\mathrm{FP,eq}}(\sigma)\\ &= \frac{1}{2} m^2\left(-1 + \frac{3K_{\frac{3}{4}}\left(\frac{m^4\pi^2}{3H^4\lambda}\right)}{K_{\frac{1}{4}}\left(\frac{m^4\pi^2}{3H^4\lambda}\right)}\right),\end{aligned} \tag{45}$$

which reduces to,

$$\langle V''(\sigma)\rangle|_{\lambda\to 0} = m^2, \tag{46}$$

$$\langle V''(\sigma)\rangle|_{m\to 0} = \frac{3\sqrt{3}\Gamma(3/4)}{\sqrt{2}\pi\Gamma(1/4)}\sqrt{\lambda}H^2 \approx 0.4\sqrt{\lambda}H^2. \tag{47}$$

To ensure slow-roll, we require

$$\langle V''(\sigma)\rangle \ll H^2. \tag{48}$$

### B. Power spectrum

To obtain isocurvature power spectrum, $P_{S_\sigma}$, we need to compute the two-point function of $\delta\rho_\sigma/\rho_\sigma$. We can write this more explicitly as,

$$\frac{\delta\rho_\sigma(\mathbf{x})}{\rho_\sigma} = \frac{\rho_\sigma(\mathbf{x}) - \langle\rho_\sigma(\mathbf{x})\rangle}{\langle\rho_\sigma(\mathbf{x})\rangle} = \frac{\rho_\sigma(\mathbf{x})}{\langle\rho_\sigma(\mathbf{x})\rangle} - 1. \tag{49}$$

where we can approximate $\rho_\sigma \approx V(\sigma)$, since $\langle V(\sigma)\rangle$ is approximately frozen, as long as Eq. (48) is satisfied. Referring to Eqs. (33) and (35), the relevant coefficient $g_n$ for $\rho_\sigma$ is determined by,

$$g_n = \frac{\int \mathrm{d}\sigma\psi_n(\sigma)\rho_\sigma\psi_0(\sigma)}{\int \mathrm{d}\sigma\psi_0(\sigma)\rho_\sigma\psi_0(\sigma)}. \tag{50}$$

For $n > 0$, the last term in Eq. (49) does not contribute because of the orthogonality of the eigenfunctions.

The eigenfunctions $\psi_n$ and the eigenvalues $\Lambda_n$ relevant for Eq. (35) can be obtained by solving the eigensystem for the potential Eq. (1). In terms of variables, $z = \lambda^{1/4}\sigma/H$ and $\alpha = m^2/(\sqrt{\lambda}H^2)$, the eigenvalue Eq. (19) can be written as [35],

TABLE I. Eigenvalues for some benchmark parameter choices corresponding to the potential in Eq. (1).

| $m^2/H^2$ | $\lambda$ | $\Lambda_2/H$ | $g_2^2$ | $\Lambda_4/H$ | $g_4^2$ |
|---|---|---|---|---|---|
| 0.2 | 0.05 | 0.16 | 1.99 | 0.37 | 0.03 |
| 0.2 | 0.07 | 0.17 | 1.98 | 0.40 | 0.05 |
| 0.2 | 0.1 | 0.18 | 1.98 | 0.44 | 0.07 |
| 0.25 | 0.05 | 0.19 | 1.99 | 0.42 | 0.02 |
| 0.25 | 0.07 | 0.20 | 1.99 | 0.45 | 0.03 |
| 0.25 | 0.1 | 0.21 | 1.98 | 0.49 | 0.05 |
| 0.3 | 0.05 | 0.22 | 1.99 | 0.48 | 0.01 |
| 0.3 | 0.07 | 0.23 | 1.99 | 0.51 | 0.02 |
| 0.3 | 0.1 | 0.24 | 1.99 | 0.54 | 0.03 |

$$\frac{\partial^2\psi_n}{\partial z^2} + \left(-\left(\frac{4\pi^2}{3}\right)^2(\alpha z + z^3)^2 + \frac{4\pi^2}{3}(\alpha + 3z^2)\right)\psi_n = -\frac{8\pi^2}{\sqrt{\lambda}}\frac{\Lambda_n}{H}\psi_n. \quad (51)$$

Given the potential in Eq. (1), the eigenfunctions are odd (even) functions of $\sigma$ for odd (even) values of $n$. Since $\rho_\sigma$ is an even function of $\sigma$, Eq. (50) implies $g_1 = 0$, and therefore, the leading coefficient is $g_2$ with the eigenvalue $\Lambda_2$ determining the first nonzero contribution to the spectral tilt. We show the numerical results for the eigenvalues for some benchmark parameter choices in Table I.

The curvature power spectrum $\Delta_\zeta^2$ depends on both $\Delta_{S_\sigma}^2$ and $f_\sigma$, as in Eq. (7). With the values of $g_n$, $\Lambda_n$ in Table I, we can compute the dimensionless power spectrum $\Delta_{S_\sigma}^2$ using Eq. (35), where we can evaluate the factor of $aH$ at the end of inflation. Furthermore, for our benchmark parameter choices, only the eigenvalue $\Lambda_2$ is relevant. Therefore, Eq. (35) can be simplified as,

$$\Delta_{S_\sigma}^2(k) \approx \frac{2g_2^2}{\pi}\Gamma\left(2 - \frac{2\Lambda_2}{H}\right)\sin\left(\frac{\pi\Lambda_2}{H}\right)\left(\frac{k}{k_{\rm end}}\right)^{2\Lambda_2/H}, \quad (52)$$

where $k_{\rm end} = a_{\rm end}H_{\rm end}$.

The precise value of $k_{\rm end}$ depends on the cosmological history after the CMB-observable modes exit the horizon. It is usually parametrized as the number of $e$-foldings $N(k) \equiv \ln(a_{\rm end}/a_k)$, where $a_k$ is the scale factor when a $k$-mode exits the horizon during inflation, defined by $k = a_k H_k$. Assuming an equation of state parameter $w$ between the end of inflation and the end of the reheating phase, we can derive the relation [36,37],

$$\frac{k}{a_0H_0} = \left(\frac{\sqrt{\pi}}{90^{1/4}}\frac{T_0}{H_0}\right)e^{-N(k)}\left(\frac{V_k^{1/2}}{\rho_{\rm end}^{1/4}M_{\rm pl}}\right)\left(\frac{\rho_{\rm RH}}{\rho_{\rm end}}\right)^{\frac{1-3w}{12(1+w)}} \times \frac{g_{*,s,0}^{1/3}g_{*,\rm RH}^{1/4}}{g_{*,\rm s,RH}^{1/3}}. \quad (53)$$

Here $g_{*,\rm RH}$ and $g_{*,\rm s,RH}$ are the effective number of degrees of freedom in the energy density and entropy density, respectively, at the end of the reheating phase; $V_k$ is the inflationary energy density when the $k$-mode exits the horizon; $\rho_{\rm end}$ and $\rho_{\rm RH}$ are the energy densities at the end of inflation and reheating, respectively. Plugging in the CMB temperature $T_0$ and the present-day Hubble parameter $H_0$, we arrive at

$$N(k) \approx 67 - \ln\left(\frac{k}{a_0H_0}\right) + \ln\left(\frac{V_k^{1/2}}{\rho_{\rm end}^{1/4}M_{\rm pl}}\right) + \frac{1-3w}{12(1+w)}\ln\left(\frac{\rho_{\rm RH}}{\rho_{\rm end}}\right) + \ln\left(\frac{g_{*,\rm RH}^{1/4}}{g_{*,\rm s,RH}^{1/3}}\right). \quad (54)$$

Significant sources of uncertainty in $N(k)$ comes from $V_k$, $\rho_{\rm end}$, $\rho_{\rm RH}$, and $w$. Furthermore, Eq. (54) assumes a standard cosmological history where following reheating, the Universe becomes radiation dominated until the epoch of matter-radiation equality. We now consider some benchmark choices with which we can evaluate $N(k)$. We set $k = a_0H_0$, assume $V_k^{1/4} = 10^{16}$ GeV, close to the current upper bound [2], $\rho_{\rm end} \simeq V_k/100$, motivated by simple slow-roll inflation models, and $w \approx 0$ [38–40].[4] Then depending on the reheating temperature, we get

$$N(k) = \begin{cases} 62, & T_{\rm RH} = 6\times10^{15}\ \text{GeV}, \\ 59, & T_{\rm RH} = 10^{11}\ \text{GeV}. \end{cases} \quad (55)$$

For the first benchmark, we have assumed an instantaneous reheating after inflation, while for the second benchmark, the reheating process takes place for an extended period of time. For these two benchmarks, $k_{\rm end} \approx 4\times10^{23}\ \text{Mpc}^{-1}$ and $10^{22}\ \text{Mpc}^{-1}$, respectively.

To determine $\Delta_\zeta^2(k)$, we also need to evaluate $f_\sigma$ as a function of time. We can express the time dependence of $f_\sigma$ in terms of $k$ in the following way. A given $k$-mode re-enters the horizon when $k = a_kH_k$, and assuming radiation domination, we get $k/k_{\rm end} = a_{\rm end}/a_k$. Since $f_\sigma$ increases with the scale factor before $\sigma$ decay, we can express $f_\sigma(t) = f_\sigma(t_d)(k_d/k)$, for $t < t_d$, where $k_d$ and $k$ are the modes that re-enter the horizon at time $t_d$ and $t$, respectively. Therefore, the final expression for the curvature power spectrum at the time of mode reentry follows from Eq. (7),

[4]The precise value of $w$ is model dependent, see, e.g., [41–46] and [47] for a review. However, this does not affect the super-horizon behavior of $\zeta_r$ and $S_\sigma$ that we described above. Instead, $w$ primarily affects the number of $e$-foldings $N(k)$ in (54). For example, using $w = 0.2(0.1)$ makes a 0.5%(0.2%) change in $N(k)$ for $T_{\rm RH} = 6\times10^{15}$ GeV in (55). For $T_{\rm RH} = 10^{11}$ GeV, using $w = 0.2(0.1)$ makes a 3%(2%) change in $N(k)$. Given these changes are less than 5%, we will use $w \approx 0$ in the rest of the analysis.

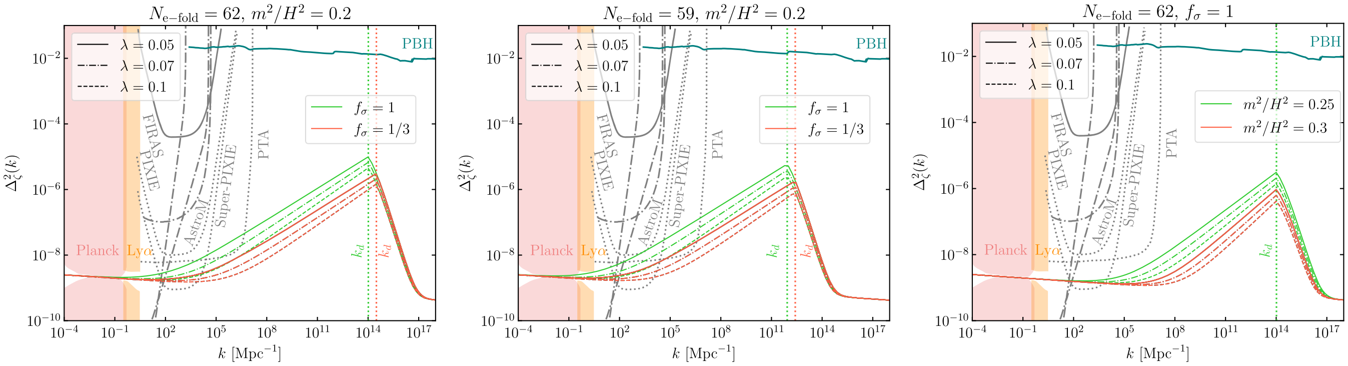


FIG. 3. Power spectrum of curvature perturbations for the benchmarks discussed above. Stochastic effects lead to a blue-tilted spectrum of $\sigma$, with larger $m$ and $\lambda$ corresponding to larger tilts, leading to faster decay as $k$ gets smaller. The blue-tilt is eventually cut off at $k_d$, the $k$-mode that reenters the horizon at the time of $\sigma$ decay. For $k$ larger than $k_d$, the fractional energy density in $\sigma$ at the time of mode-reentry is smaller. Correspondingly, $\Delta_\zeta^2$ gets suppressed. Eventually, for very large $k$, the effects of $\sigma$ become negligible, and $\Delta_\zeta^2$ reverts back to its standard, slightly red-tilted behavior. A smaller value of $f_\sigma(k_d)$, the fractional energy density at the time $\sigma$ decay, suppresses the effect of $\sigma$ to $\Delta_\zeta^2$, and hence leads to a suppressed peak. This mechanism predicts signatures in CMB spectral distortion measurements [48], especially in Super-PIXIE [49], along with Pulsar Timing Array (PTA) probes for enhanced DM substructure [50], and precision astrometry probes (AstroM) [51]. We also show constraints from FIRAS [52] and nonobservation of primordial black holes (PBH) [5].

$$\Delta_\zeta^2(k) = \begin{cases} \Delta_{\zeta_r}^2(k) + \left(\frac{f_\sigma(t_d)}{4+3f_\sigma(t_d)}\right)^2 \Delta_{S_\sigma}^2(k), & k < k_d, \\ \Delta_{\zeta_r}^2(k) + \left(\frac{f_\sigma(t_d)(k_d/k)}{4+3f_\sigma(t_d)(k_d/k)}\right)^2 \Delta_{S_\sigma}^2(k), & k > k_d. \end{cases} \tag{56}$$

To determine the scale $k_d$, we consider the benchmarks discussed above, along with some additional choices for other parameters.

*a. Benchmark 1*. We focus on the first benchmark in Eq. (55). For $m^2 = 0.2H^2$ and $\lambda \simeq 0.05$–$0.1$, we get $\langle V(\sigma)\rangle \approx 0.02H^4$ from Eq. (41), implying $\langle V(\sigma)\rangle/V_k \approx 3\times 10^{-12}$ for $H = 5\times 10^{13}$ GeV. Assuming instantaneous reheating, and $\rho_{\text{end}} \simeq V_k/100$, we see $f_\sigma \simeq 1$ for $a \simeq (1/3)\times 10^{10} a_{\text{end}}$. As benchmarks, we assume $\sigma$ decays when $f_\sigma = 1$ and $1/3$. Using $k_{\text{end}} \approx 4\times 10^{23}$ Mpc$^{-1}$, we can then evaluate $k_d \approx 10^{14}$ Mpc$^{-1}$ and $k_d \approx 3\times 10^{14}$ Mpc$^{-1}$, respectively. The result for the curvature power spectrum with these choices is shown in Fig. 3 (left).

*b. Benchmark 2*. We now discuss the second benchmark in Eq. (55). We again choose $m^2 = 0.2H^2$ and $\lambda \simeq 0.05$–$0.1$, for which we get $\langle V(\sigma)\rangle \approx 0.02H^4$ from Eq. (41). This implies $\langle V(\sigma)\rangle/V_k \approx 3\times 10^{-12}$ for $H = 5\times 10^{13}$ GeV, as before. The rest of the parameters can be derived in an analogous way, with one difference. During the reheating epoch, with our assumption $w \approx 0$, $f_\sigma$ does not grow with the scale factor since the dominant energy density of the Universe is also diluting as matter. Accounting for this gives $k_d \approx 8\times 10^{11}$ Mpc$^{-1}$ and $k_d \approx 3\times 10^{12}$ Mpc$^{-1}$, for $f_\sigma = 1$ and $1/3$, respectively, with the resulting curvature power spectrum shown in Fig. 3 (center).

*c. Benchmark 3*. This is same as the first benchmark discussed above, except we focus on $m^2 = 0.25H^2$ and $0.3H^2$ along with $f_\sigma = 1$. The result is shown in Fig. 3 (right).

We note that for all three cases, the power spectrum does not become as large as to give rise to PBH. It can also be checked that the correction to the large-scale power spectrum, relevant for the CMB, from the enhanced small-scale power spectrum, is small. In fact, repeating the argument of [53], we find

$$\delta P_\zeta(k_L) \sim \frac{\Delta_\zeta^4}{k_s^3} \sim \frac{\Delta_\zeta^4}{\Delta_{\zeta,\text{CMB}}^2} \frac{k_L^3}{k_s^3} P_\zeta(k_L). \tag{57}$$

For $\Delta_\zeta^2 \sim 10^{-5}$ and $k_s \sim 10^{14}$ Mpc$^{-1}$, as in Fig. 3 (left) near the peak, we have

$$\delta P_\zeta(k_L) \sim 10^{-46} P_\zeta(k_L), \tag{58}$$

for $k_L \sim 10^{-1}$ Mpc$^{-1}$ and $\Delta_{\zeta,\text{CMB}}^2 \sim 10^{-9}$ (corresponding to a typical scale probed by the CMB).

## V. GRAVITATIONAL WAVE SIGNATURE

### A. Secondary gravitational waves from scalar curvature perturbation

We now review how large primordial curvature perturbations can source GW at the second order in perturbation theory [54–57] (for a review see [4]). We then evaluate the GW spectrum sourced by $\Delta_\zeta^2$ computed in Sec. IV. We start our discussion with a brief review of the essential relations, following [58], and expand the discussion further in

Appendix A. For some recent work on scalar-induced gravitational waves, see, e.g., Refs. [59,60].

We can write a tensor perturbation in Fourier space as,

$$h_{ij}(\tau,\mathbf{x}) = \sum_{\lambda=+,\times}\int \frac{\mathrm{d}^3k}{(2\pi)^3} e^{i\mathbf{k}\cdot\mathbf{x}}\epsilon_{ij}^{\lambda}(\mathbf{k})h_\lambda(\tau,\mathbf{k}), \tag{59}$$

where $\epsilon_{ij}^{\lambda=\{+,\times\}}(\mathbf{k})$ are polarization tensors:

$$\epsilon_{ij}^{+}(\mathbf{k}) = \frac{1}{\sqrt{2}}(\mathrm{e}_{1,i}(\mathbf{k})\mathrm{e}_{1,j}(\mathbf{k}) - \mathrm{e}_{2,i}(\mathbf{k})\mathrm{e}_{2,j}(\mathbf{k})), \tag{60}$$

$$\epsilon_{ij}^{\times}(\mathbf{k}) = \frac{1}{\sqrt{2}}(\mathrm{e}_{1,i}(\mathbf{k})\mathrm{e}_{2,j}(\mathbf{k}) + \mathrm{e}_{2,i}(\mathbf{k})\mathrm{e}_{1,j}(\mathbf{k})), \tag{61}$$

with $\mathrm{e}_{1,2}$ the orthonormal bases spanning the plane transverse to $\mathbf{k}$. The equation of motion determining the generation and evolution of GW is given by

$$h_\lambda''(\tau,\mathbf{k}) + 2\mathcal{H}h_\lambda'(\tau,\mathbf{k}) + k^2h_\lambda(\tau,\mathbf{k}) = 4\mathcal{S}_\lambda(\tau,\mathbf{k}), \tag{62}$$

where $'$ denotes derivative with respect to the conformal time $\tau$ and $\mathcal{H} = a'/a$ is the conformal Hubble parameter. The second-order (in scalar metric perturbation $\Phi$) source term is given by[5]

$$\mathcal{S}_\lambda(\tau,\mathbf{k}) = \int \frac{\mathrm{d}^3q}{(2\pi)^3}\frac{Q_\lambda(\mathbf{k},\mathbf{q})}{3(1+w)}[2(5+3w)\Phi_\mathbf{p}\Phi_\mathbf{q} + \tau^2(1+3w)^2\Phi_\mathbf{p}'\Phi_\mathbf{q}' + 2\tau(1+3w)(\Phi_\mathbf{p}\Phi_\mathbf{q}' + \Phi_\mathbf{p}\Phi_\mathbf{q}')]. \tag{64}$$

We have defined $\mathbf{p}\equiv\mathbf{k}-\mathbf{q}$, $\Phi_\mathbf{k}\equiv\Phi(\tau,\mathbf{k})$, and a projection operator $Q_\lambda(\mathbf{k},\mathbf{q})$:

$$Q_\lambda(\mathbf{k},\mathbf{q}) \equiv \epsilon_\lambda^{ij}(\mathbf{k})q_iq_j. \tag{65}$$

The metric perturbation $\Phi(\tau,\mathbf{k})$ can be written in terms of the primordial curvature perturbation $\zeta(\mathbf{k})$,

$$\Phi(\tau,\mathbf{k}) = \frac{3+3w}{5+3w}T_\Phi(k\tau)\zeta(\mathbf{k}), \tag{66}$$

via a transfer function $T_\Phi(k\tau)$ which depends on $w$. With the above quantities, one can now solve Eq. (62) using the Green function method,[6]

$$h_\lambda(\tau,\mathbf{k}) = \frac{4}{a(\tau)}\int_{\tau_0}^{\tau}\mathrm{d}\bar{\tau}G_\mathbf{k}(\tau,\bar{\tau})a(\bar{\tau})\mathcal{S}_\lambda(\bar{\tau},\mathbf{k}). \tag{67}$$

Using the solutions of Eq. (62), the power spectrum $P_\lambda(\tau,k)$, defined via,

$$\langle h_{\lambda_1}(\tau,\mathbf{k}_1)h_{\lambda_2}(\tau,\mathbf{k}_2)\rangle \equiv (2\pi)^3\delta_{\lambda_1\lambda_2}\delta^3(\mathbf{k}_1+\mathbf{k}_2)P_{\lambda_1}(\tau,k_1), \tag{68}$$

can be written as,

$$\langle h_{\lambda_1}(\tau,\mathbf{k}_1)h_{\lambda_2}(\tau,\mathbf{k}_2)\rangle = 16\int\frac{\mathrm{d}^3q_1}{(2\pi)^3}\frac{\mathrm{d}^3q_2}{(2\pi)^3}Q_{\lambda_1}(\mathbf{k}_1,\mathbf{q}_1)Q_{\lambda_2}(\mathbf{k}_2,\mathbf{q}_2)I(|\mathbf{k}_1-\mathbf{q}_1|,q_1,\tau_1) \times I(|\mathbf{k}_2-\mathbf{q}_2|,q_2,\tau_2)\langle\zeta(\mathbf{q}_1)\zeta(\mathbf{k}_1-\mathbf{q}_1)\zeta(\mathbf{q}_2)\zeta(\mathbf{k}_2-\mathbf{q}_2)\rangle. \tag{69}$$

Here

$$I(p,q,\tau) = \frac{1}{a(\tau)}\int_{\tau_0}^{\tau}\mathrm{d}\bar{\tau}\,G_\mathbf{k}(\tau,\bar{\tau})a(\bar{\tau})f(p,q,\bar{\tau}), \tag{70}$$

and

$$\frac{(5+3w)^2}{3(1+w)}f(p,q,\tau) = 2(5+3w)T_\Phi(p\tau)T_\Phi(q\tau) + \tau^2(1+3w)^2T_\Phi'(p\tau)T_\Phi'(q\tau) + 2\tau(1+3w)[T_\Phi(p\tau)T_\Phi'(q\tau) + T_\Phi'(p\tau)T_\Phi(q\tau)]. \tag{71}$$

[5]We parametrize the scalar metric fluctuations, for vanishing anisotropic stress, as

$$\mathrm{d}s^2 = -(1+2\Phi)\mathrm{d}t^2 + a^2(1-2\Phi)\delta_{ij}\mathrm{d}x^i\mathrm{d}x^j \tag{63}$$

[6]Scale factors appearing in the $I$ integral as $a(\bar{\tau})/a(\tau)$ are the artifact of $G_\mathbf{k}(\tau,\bar{\tau})$ being Green's function of the new variable $v(\tau,\mathbf{k}) = ah(\tau,\mathbf{k})$ and not $h_\lambda$ itself; see Appendix A 2.

where $T'_\Phi(p\tau) = \partial T_\Phi(p\tau)/\partial\tau$. We note that the power spectrum is sourced by the four-point correlation function of superhorizon curvature perturbations, and is further modified by the subhorizon evolution as encapsulated in $I(p, q, \tau)$.

The four-point function in Eq. (69) has both disconnected and connected contributions, from the scalar power spectrum and trispectrum, respectively. The connected contribution usually contributes in a subdominant way compared to the disconnected piece in determining total GW energy density; see [61] for a general argument.[7] Therefore, in the following, we focus only on the disconnected contribution, which can be written as

$$P_\lambda(\tau, k)|_{\rm d} = 32 \int \frac{{\rm d}^3 q}{(2\pi)^3} Q_\lambda(\mathbf{k}, \mathbf{q})^2 I(|\mathbf{k}-\mathbf{q}|, q, \tau)^2 \times P_\zeta(q) P_\zeta(|\mathbf{k}-\mathbf{q}|). \tag{72}$$

For a derivation of this formula see Appendix A 3.

GW signal strength can be characterized by SGWB energy density per unit logarithmic interval of frequency and normalized to the total energy density [64],

$$h^2\Omega_{\rm GW} = \frac{1}{\rho_{\rm tot}} \frac{{\rm d}\rho_{\rm GW}}{{\rm d}\log f} \tag{73}$$

where the present day Hubble parameter is given by $H_0 = 100h$ km/s/Mpc and $\rho_{\rm tot} = 3M_{\rm pl}^2 H_0^2$ is the critical energy density in terms of the reduced Planck mass $M_{\rm pl} \approx 2.4 \times 10^{18}$ GeV. The total energy density $\rho_{\rm GW}$ is given by,

$$\rho_{\rm GW} = \frac{M_{\rm pl}^2}{4} \int {\rm d}\ln k \frac{k^3}{16\pi^2} \times \sum_\lambda \left( \langle \dot h_\lambda(t, \mathbf{k}) \dot h_\lambda(t, -\mathbf{k})\rangle' + \frac{k^2}{a^2} \langle h_\lambda(t, \mathbf{k}) h_\lambda(t, -\mathbf{k})\rangle' \right), \tag{74}$$

with the primes denoting the fact that momentum-conserving delta functions are factored out, $\langle h_\lambda(t, \mathbf{k}) h_\lambda(t, \mathbf{k}')\rangle = (2\pi)^3 \delta^3(\mathbf{k} + \mathbf{k}') \langle h_\lambda(t, \mathbf{k}) h_\lambda(t, -\mathbf{k})\rangle'$. Approximating $\dot h_\lambda(t, \mathbf{k}) \approx (k/a) h_\lambda(t, \mathbf{k})$, we can simplify to get,[8]

$$\Omega_{\rm GW} = \frac{1}{48} \left( \frac{k}{a(\tau)H(\tau)} \right)^2 \sum_{\lambda=+,\times} \Delta_\lambda^2(\tau, k), \tag{75}$$

where $\Delta_\lambda^2(\tau, k) = (k^3/(2\pi^2)) P_\lambda(\tau, k)$.

[7] See also [58,62,63] for examples where the connected contribution can be important.

[8] Note that we are using the convention at which the spatial part of the metric is given by $a^2(\delta_{ij} + h_{ij}/2){\rm d}x^i {\rm d}x^j$. If we were using an alternative convention $a^2(\delta_{ij} + h_{ij}){\rm d}x^i {\rm d}x^j$, then the factor of $1/48$ would be replaced by $1/12$ as in Refs. [56,64].

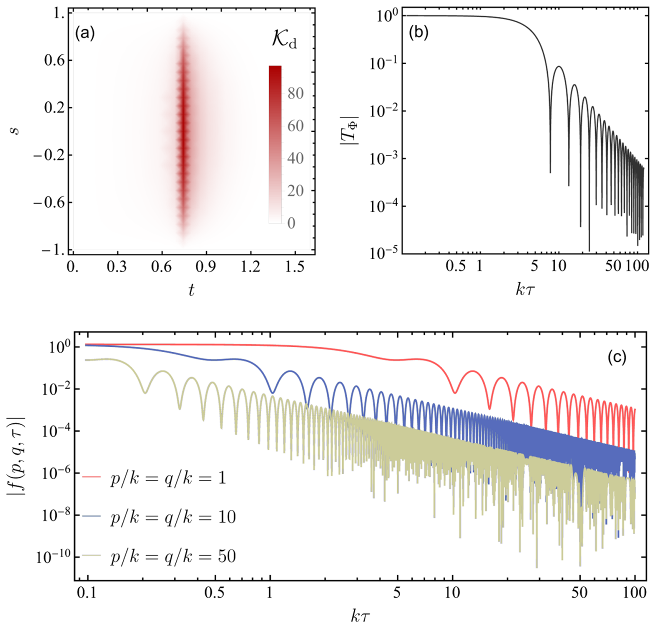


FIG. 4. (a) The kernel function from Eq. (76). We note a clear resonance contribution from $t \simeq 0.7$ corresponding to $u + v \simeq \sqrt{3}$. (b) The transfer function $T_\Phi$. (c) Function $f(p, q, \tau)$ as in Eq. (71). We see that for the scalar modes that enter the horizon earlier, with $p, q > k$, this function is more suppressed as expected from the behavior of the transfer function.

The above expression can be rewritten in form convenient for numerical evaluation (see Appendix A 4 for a derivation),[9]

$$\Omega_{\rm GW}(k) = \frac{2}{48\alpha^2} \int_0^\infty {\rm d}t \int_{-1}^1 {\rm d}s\, \mathcal{K}_{\rm d}(u, v) \Delta_\zeta^2(uk) \Delta_\zeta^2(vk) \tag{76}$$

where $u = |\mathbf{k} - \mathbf{q}|/k = p/k, v = q/k, s = u - v, t = u + v - 1$, and $\mathcal{K}_{\rm d}$ is the kernel function following from manipulating the integrand of Eq. (72). This kernel function is illustrated in fig. 4a.

We now focus on the scenario where GW is generated during a radiation dominated epoch and set $w = 1/3$. We can then write (see Appendix A 1 for details),

$$T_\Phi(k\tau) = \frac{9\sqrt{3}}{(k\tau)^3} \left( \sin\frac{k\tau}{\sqrt{3}} - \frac{k\tau}{\sqrt{3}} \cos\frac{k\tau}{\sqrt{3}} \right), \tag{77}$$

and plot this function in Fig. 4(b). We note that after entering the horizon, modes start to oscillate and decay, and as a result, the subhorizon modes do not significantly contribute to GW generation. In Fig. 4(c), we confirm that at any given time $f(p, q, \tau)$ is suppressed for shorter modes

[9] Note that the integration variable $u$ and $v$ are swapped with $t$ and $s$ since in the $t - s$ space, integration limits are independent of the integration variables.

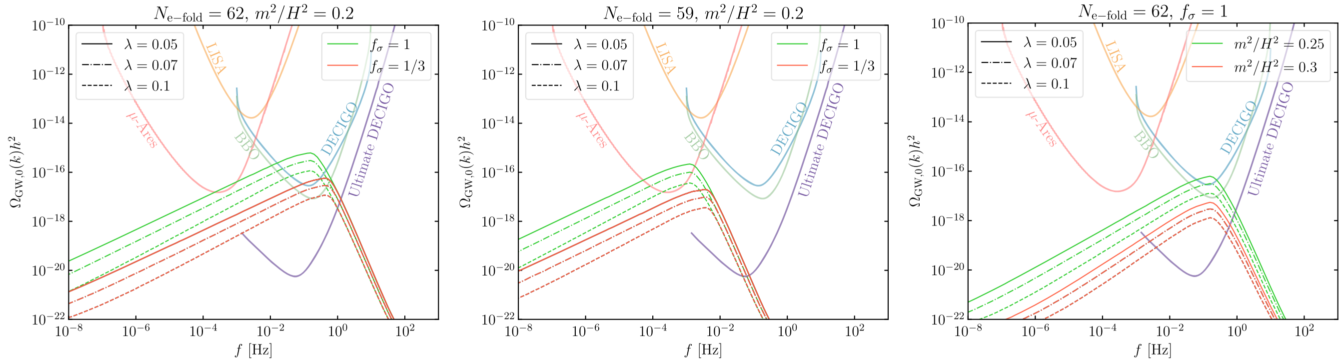


FIG. 5. Gravitational wave spectrum for the benchmarks discussed in Fig. 3. We notice that the number of $e$-folds after CMB-observable modes exited the horizon determines the peak frequency of the spectrum, and correspondingly, different detectors can be sensitive to the signal. Although a similarly peaked spectrum would appear in the context of cosmological phase transitions (PT), the low-frequency tail of this GW spectrum is different from the usual $f^3$ tail. While in the context of PT the $f^3$ scaling originates due to causality and superhorizon behavior of fluctuations, in our scenario, the $f$-scaling is determined by $\sigma$ mass. The differing frequency dependence can then be used to discriminate between the two classes of signals.

that have reentered the horizon earlier. Finally, the green function is given by (see Appendix A 2 for details)

$$G_{\mathbf{k}}(\tau, \bar{\tau}) = \frac{\sin[k(\tau - \bar{\tau})]}{k}. \tag{78}$$

With these expressions, we can obtain a physical understanding of GW generation via Eq. (72). The Green function, given in Eq. (78), is an oscillatory function of time whose frequency is $k$. The quantity $f(p, q, \tau)$ is also an oscillatory and decaying function of time (see fig. 4c), inheriting these properties from the transfer function (77). Therefore, the dominant contribution to the integral (70) is a resonant contribution when the momentum of the produced GW is of the same order as the momentum of the scalar modes, i.e., $k \sim p \sim q$. In particular, the resonant point is at $u + v \simeq \sqrt{3}$ [61] as shown in Fig. 4(a). GW generation is suppressed in other parts of the phase space. For example, the source term, which contains gradients of the curvature perturbation [55], is suppressed by small derivatives if any of the wave numbers $p$, $q$ of $\zeta$ is much smaller than $k$. On the other hand, if $p$, $q$ are much larger than $k$, then the scalar modes would have decayed significantly after entering the horizon by the time $k \sim H$, and thus the production of GW with momentum $k$ gets suppressed.

To obtain the final result for $\Omega_{\rm GW}$, we note that the GW comoving wave number $k$ is related to the present-day, redshifted frequency $f$ of the generated GW via

$$f = f_* \left(\frac{a_*}{a_0}\right) = \frac{k}{2\pi} \simeq 1.5 \text{ mHz} \left(\frac{k}{10^{12}\text{ Mpc}^{-1}}\right), \tag{79}$$

where $f_*$ and $a_*$ are respectively the frequency and the scale factor at the time of GW generation. Using these expressions, we arrive at our final result, shown in Fig. 5, for the same benchmark choices discussed in Fig. 3. We see that stochastic effects can naturally give rise to a large enough SGWB, within the sensitivity range of DECIGO, BBO, $\mu$-Ares, and Ultimate DECIGO [65–67].

## VI. CONCLUSION

In this work, we have discussed an early Universe scenario containing a light spectator field, along with an inflaton field. The fluctuations of the inflaton are red-tilted and explain the observed fluctuations in the CMB and LSS. On the other hand, the spectator field $\sigma$ naturally acquires a blue-tilted power spectrum. This blue-tilted power spectrum is eventually cut-off at very small scales since when such small-scale modes enter the horizon, the spectator field contributes subdominantly to the total energy density. As a consequence, primordial black holes are not produced in this scenario. Overall, this mechanism of generating a blue-tilted spectrum works for any generic inflaton potential and does not require any particular fine-tuning or structure such as an inflection point or a bump on the potential or an ultra slow-roll phase.

The blue-tilted spectrum gives rise to large curvature perturbations at small scales. These, in turn, source a stochastic gravitational wave background (SGWB) when the perturbations reenter the horizon. Focusing on some benchmark choices for the number of $e$-foldings and spectator field potential, we have shown that this scenario predicts observable gravitational waves at future detectors operating in $10^{-5}$ Hz to 10 Hz range, with strengths $\Omega_{\rm GW}h^2 \simeq 10^{-20}$–$10^{-15}$.

There are various interesting future directions. In particular, we have worked in a regime where $\sigma$ does not dominate the energy density during the cosmological history. It would be interesting to explore the consequences of an early matter-dominated era caused by the $\sigma$ field.

We have also seen that the low-frequency scaling of the SGWB spectrum depends on the mass and coupling of $\sigma$ and is generally different from the $f^3$-scaling expected in the context of cosmological PT, or $f^{2/3}$-scaling expected in the context of binary mergers. This different frequency dependence can be used to identify the origin of an SGWB, and distinguish between various cosmological or astrophysical contributions. Along these lines, it would be interesting to carry out a quantitative analysis to understand how well we can separate any two frequency dependencies, for example, by doing a Fisher analysis.

*Note added.* While we were finishing this work, results from NANOGrav [68], EPTA, InPTA [69,70], PPTA [71], CPTA [72] appeared. Secondary gravitational waves from the scalar perturbation can in principle give rise to the signal [73,74]. Such scalar perturbations could be generated in a model similar to the one considered in this paper. However, the frequency dependence of $\Omega_{\rm GW}h^2$ determined by the NANOGrav result is [68] $1.8 \pm 0.6$. We note that for a free field with mass $m$, the frequency dependence of $\Omega_{\rm GW}h^2$ is given by, $4m^2/(3H^2)$. So for the central value, one would naively infer $m^2/H^2 = 1.4$. Therefore to interpret it in terms of a free field, we require a mass bigger than the Hubble scale. However, since for larger than Hubble-scale masses, the stochastic effects are not efficient, one may have to go beyond the stochastic scenario to explain the NANOGrav observations. We could instead consider a regime in which the misalignment contribution is important [13,14]. We will leave a detailed analysis of this scenario to future work.

## ACKNOWLEDGMENTS

We thank Keisuke Harigaya, Andrew Long, and Neal Weiner for their helpful discussions. R. E. is supported in part by the University of Maryland Quantum Technology Center. S. K. is supported in part by the National Science Foundation (NSF) Grant No. PHY-1915314 and the U.S. DOE Contract No. DE-AC02-05CH11231. S. K. thanks Aspen Center for Physics, supported by NSF Grant No. PHY-2210452, for hospitality while this work was in progress. The research of A. M. is supported by the U.S. Department of Energy, Office of Science, Office of Workforce Development for Teachers and Scientists, Office of Science Graduate Student Research (SCGSR) program under contract number DESC0014664. L. T. W. is supported by the DOE grant No. DE-SC0013642.

## APPENDIX A: SCALAR-INDUCED GRAVITATIONAL WAVES: TECHNICAL DETAILS

In this appendix, we review the formalism relevant to computing GW energy density for the sake of completeness, following the notation and analysis of Ref. [58].

### 1. Transfer functions

The equation of motion for the scalar perturbation $\Phi$ in the absence of isocurvature perturbations is,

$$\Phi''(\tau,\mathbf{k}) + 3(1+c_s^2)\mathcal{H}\Phi'(\tau,\mathbf{k}) + c_s^2 k^2 \Phi(\tau,\mathbf{k}) = 0, \tag{A1}$$

where $c_s^2 \simeq w$ is the sound speed of the fluid. Defining dimensionless parameter $y = \sqrt{w}k\tau$, we rewrite this equation as

$$\frac{\mathrm{d}^2\Phi(y,\mathbf{k})}{\mathrm{d}y^2} + \frac{6(1+w)}{1+3w}\frac{1}{y}\frac{\mathrm{d}\Phi(y,\mathbf{k})}{\mathrm{d}y} + \Phi(y,\mathbf{k}) = 0. \tag{A2}$$

A general solution is given by,

$$\Phi(y,\mathbf{k}) = y^{-\gamma}[C_1(\mathbf{k})J_\gamma(y) + C_2(\mathbf{k})Y_\gamma(y)], \tag{A3}$$

where $J_\gamma$ and $Y_\gamma$ are spherical Bessel functions of the first and second kind, respectively, of order $\gamma$

$$\gamma = \frac{3(1+w)}{1+3w} - 1. \tag{A4}$$

In the radiation dominated era, in which $w = 1/3 \to \gamma = 1$, we have

$$\Phi(y,\mathbf{k}) = \frac{1}{y^2}\left[C_1(\mathbf{k})\left(\frac{\sin y}{y} - \cos y\right) + C_2(\mathbf{k})\left(\frac{\cos y}{y} + \sin y\right)\right]. \tag{A5}$$

We can deduce the initial conditions of this solution by considering the early-time limit $k\tau \ll 1$,

$$\frac{\sin y}{y} - \cos y \simeq \frac{y^2}{3} \quad \text{and} \quad \frac{\cos y}{y} + \sin y \simeq \frac{1}{y}. \tag{A6}$$

The first term ($\propto C_1$) is then constant in this limit, while the second term ($\propto C_2$) decays as $1/y^3 \sim 1/a^3$. We can therefore assume the initial conditions,

$$C_1(\mathbf{k}) = 2\zeta(\mathbf{k}), \qquad C_2(\mathbf{k}) = 0, \tag{A7}$$

which gives a particular solution,

$$\Phi(\tau,\mathbf{k}) = \frac{2}{3}\zeta(\mathbf{k})\frac{3}{y^2}\left(\frac{\sin y}{y} - \cos y\right), \tag{A8}$$

resulting in the transfer function, via (66),

$$T_\Phi(k\tau) = \frac{3}{(k\tau/\sqrt{3})^3}\left(\sin\frac{k\tau}{\sqrt{3}} - \frac{k\tau}{\sqrt{3}}\cos\frac{k\tau}{\sqrt{3}}\right). \tag{A9}$$

We can now see the distinct behavior of superhorizon ($k\tau \ll 1$) and subhorizon ($k\tau \gg 1$) modes in the radiation dominated era. While the superhorizon modes freeze via our analysis above, the subhorizon modes oscillate and damp as $\sim \cos k\tau/(k\tau)^2$.

In the matter dominated era, $w = 0$ and the equation of motion for $\Phi$ becomes,

$$\Phi''(\tau, \mathbf{k}) + 3\mathcal{H}\Phi'(\tau, \mathbf{k}) = 0, \tag{A10}$$

leading to a constant transfer function.

### 2. Green's function and GW solution

In this subsection, we discuss in detail the solutions to Eq. (62), which is derived using the second-order Einstein equation, $G_{ij}^{(2)} = 8\pi G T_{ij}^{(2)}$, for second-order tensor and first-order scalar contributions. We neglect scalar anisotropic stress, and second-order vector and scalar perturbations. In other words, we use the following perturbed FLRW metric in the Newtonian gauge,

$$\mathrm{d}s^2 = -(1+2\Phi)\mathrm{d}t^2 + a^2\left((1-2\Phi)\delta_{ij} + \frac{1}{2}h_{ij}\right)\mathrm{d}x^i\mathrm{d}x^j, \tag{A11}$$

assuming a perfect fluid energy-momentum tensor with equation of state $w$. Using lower order solutions and projecting out spatial indices using polarization tensors, i.e. $\epsilon_\lambda^{ij} T_{ij} = T_\lambda$ for any tensor $T$, we recover (62). For simplicity, we define a new variable $v(\tau, \mathbf{k}) = a h_\lambda(\tau, \mathbf{k})$, which gives the equation of motion for $v(\tau, \mathbf{k})$,

$$v''(\tau, \mathbf{k}) + \left[k^2 - \frac{a''(\tau)}{a(\tau)}\right] v(\tau, \mathbf{k}) = 4a(\tau)\mathcal{S}_\lambda(\tau, \mathbf{k}). \tag{A12}$$

We need the two homogeneous solutions of this equation $v_1(\tau)$ and $v_2(\tau)$ to construct the Green's function,

$$G_{\mathbf{k}}(\tau, \bar{\tau}) = \frac{v_1(\tau)v_2(\bar{\tau}) - v_1(\bar{\tau})v_2(\tau)}{v_1'(\bar{\tau})v_2(\bar{\tau}) - v_1(\bar{\tau})v_2'(\bar{\tau})}. \tag{A13}$$

For each $\mathbf{k}$ we have

$$v_{1,2}''(\tau) + \left[k^2 - \frac{a''(\tau)}{a(\tau)}\right] v_{1,2}(\tau) = 0 \tag{A14}$$

which, using $a \propto \tau^\alpha$ and $x = k\tau$, leads to

$$\frac{\mathrm{d}^2 v_{1,2}(x)}{\mathrm{d}x^2} + \left[1 - \frac{\alpha(\alpha-1)}{x^2}\right] v_{1,2}(x) = 0, \tag{A15}$$

where $\alpha = 2/(1+3w)$. The solutions are

$$v_1(x) = \sqrt{x} J_{\alpha-1/2}(x) \tag{A16}$$

$$v_2(x) = \sqrt{x} Y_{\alpha-1/2}(x) \tag{A17}$$

where $J_{\alpha-1/2}$ and $Y_{\alpha-1/2}$ are again spherical Bessel functions of first and second kind, respectively. We note that

$$\frac{\mathrm{d}v_1}{\mathrm{d}x} = \frac{\alpha}{\sqrt{x}} J_{\alpha-1/2}(x) - \sqrt{x} J_{\alpha+1/2} \tag{A18}$$

$$\frac{\mathrm{d}v_2}{\mathrm{d}x} = \frac{\alpha}{\sqrt{x}} Y_{\alpha-1/2}(x) - \sqrt{x} Y_{\alpha+1/2}. \tag{A19}$$

Now, we can calculate the expression in the denominator of the Green's function,

$$\begin{aligned} v_1'(x)v_2(x) - v_1(x)v_2'(x) &= kx[J_{\alpha-1/2}(x)Y_{\alpha+1/2}(x) \\ &\quad - J_{\alpha+1/2}(x)Y_{\alpha-1/2}(x)] \\ &= -\frac{2}{\pi}. \end{aligned} \tag{A20}$$

The second equality can be checked explicitly via *Mathematica*. Thus, (A13) simplifies to

$$\begin{aligned} G_{\mathbf{k}}(\tau, \bar{\tau}) = \frac{\pi}{2}\sqrt{\tau\bar{\tau}}[&J_{\alpha-1/2}(k\bar{\tau})Y_{\alpha-1/2}(k\tau) \\ &-J_{\alpha-1/2}(k\tau)Y_{\alpha-1/2}(k\bar{\tau})]. \end{aligned} \tag{A21}$$

In the radiation dominated era, $\alpha = 1$, and so,

$$G_{\mathbf{k}}(\tau, \bar{\tau}) = \frac{\sin k(\tau - \bar{\tau})}{k}, \tag{A22}$$

where we have used (A54) to replace Bessel functions of order 1/2. In the matter dominated era we have $\alpha = 2$, and so,

$$\begin{aligned} G_{\mathbf{k}}(\tau, \bar{\tau}) = \frac{1}{k}\Bigg[&\left(\frac{\bar{\tau} - \tau}{\tau\bar{\tau}}\right)\cos k(\tau - \bar{\tau}) \\ &+ \left(\frac{1/k^2 - \tau\bar{\tau}}{\tau\bar{\tau}}\right)\sin k(\tau - \bar{\tau})\Bigg]. \end{aligned} \tag{A23}$$

where we have again used (A54) to replace Bessel functions of order 3/2.

Having calculated the Green's functions, we can now write the solution for $h_\lambda(\tau, \mathbf{k})$ in the form of (67).

### 3. Connected and disconnected 4-point correlation function

The primordial 4-point correlation function of $\zeta$ can be written in terms of disconnected and connected pieces

$$\begin{aligned} \langle\zeta(\mathbf{k}_1)\zeta(\mathbf{k}_2)\zeta(\mathbf{k}_3)\zeta(\mathbf{k}_4)\rangle &= \langle\zeta(\mathbf{k}_1)\zeta(\mathbf{k}_2)\zeta(\mathbf{k}_3)\zeta(\mathbf{k}_4)\rangle_{\mathrm{d}} \\ &\quad + \langle\zeta(\mathbf{k}_1)\zeta(\mathbf{k}_2)\zeta(\mathbf{k}_3)\zeta(\mathbf{k}_4)\rangle_{\mathrm{c}}, \end{aligned} \tag{A24}$$

where

$$\begin{aligned}\langle\zeta(\mathbf{k}_1)\zeta(\mathbf{k}_2)\zeta(\mathbf{k}_3)\zeta(\mathbf{k}_4)\rangle_{\rm d} = (2\pi)^6\delta^3(\mathbf{k}_1+\mathbf{k}_2)\delta^3(\mathbf{k}_3+\mathbf{k}_4)P_\zeta(k_1)P_\zeta(k_3)\\ +(2\pi)^6\delta^3(\mathbf{k}_1+\mathbf{k}_3)\delta^3(\mathbf{k}_2+\mathbf{k}_4)P_\zeta(k_1)P_\zeta(k_2)\\ +(2\pi)^6\delta^3(\mathbf{k}_1+\mathbf{k}_4)\delta^3(\mathbf{k}_2+\mathbf{k}_4)P_\zeta(k_1)P_\zeta(k_4),\end{aligned} \tag{A25}$$

and

$$\langle\zeta(\mathbf{k}_1)\zeta(\mathbf{k}_2)\zeta(\mathbf{k}_3)\zeta(\mathbf{k}_4)\rangle_{\rm c} = (2\pi)^3\delta^3(\mathbf{k}_1+\mathbf{k}_2+\mathbf{k}_3+\mathbf{k}_4)\mathcal{T}(\mathbf{k}_1,\mathbf{k}_2,\mathbf{k}_3,\mathbf{k}_4). \tag{A26}$$

Here, $P_\zeta(k)$ and $\mathcal{T}(\mathbf{k}_1,\mathbf{k}_2,\mathbf{k}_3,\mathbf{k}_4)$ are the scalar power spectrum and trispectrum, respectively. We focus on the disconnected contribution below. The relevant 4-point correlation function for the GW power spectrum (69) is

$$\langle\zeta(\mathbf{q}_1)\zeta(\mathbf{k}_1-\mathbf{q}_1)\zeta(\mathbf{q}_2)\zeta(\mathbf{k}_2-\mathbf{q}_2)\rangle_{\rm d} = (2\pi)^6\delta^3(\mathbf{k}_1+\mathbf{k}_2)[\delta^3(\mathbf{q}_1+\mathbf{q}_2)+\delta^3(\mathbf{k}_1+\mathbf{q}_2-\mathbf{q}_1)]P_\zeta(q_1)P_\zeta(|\mathbf{k}_1-\mathbf{q}_1|). \tag{A27}$$

The two terms in the above expressions are equivalent when substituted in the integrand of (69). The second term can be manipulated as

$$\begin{aligned}&\delta^3(\mathbf{k}_1+\mathbf{k}_2)\delta^3(\mathbf{k}_1+\mathbf{q}_2-\mathbf{q}_1)Q_{\lambda_1}(\mathbf{k}_1,\mathbf{q}_1)Q_{\lambda_2}(\mathbf{k}_2,\mathbf{q}_2)I(|\mathbf{k}_1-\mathbf{q}_1|,q_1,\tau)I(|\mathbf{k}_2-\mathbf{q}_2|,q_2,\tau)\\ &\quad= Q_{\lambda_1}(\mathbf{k}_1,\mathbf{q}_1)Q_{\lambda_2}(-\mathbf{k}_1,\mathbf{q}_1-\mathbf{k}_1)I(|\mathbf{k}_1-\mathbf{q}_1|,q_1,\tau)I(q_1,|\mathbf{k}_1-\mathbf{q}_1|,\tau)\\ &\quad= Q_{\lambda_1}(\mathbf{k}_1,\mathbf{q}_1)^2 I(|\mathbf{k}_1-\mathbf{q}_1|,q_1,\tau)^2\end{aligned} \tag{A28}$$

which is the same result we get from the first term. Here we have used identities given in eqs. (A51)–(A53). Thus, the disconnected GW power spectrum is given by (72).

#### 4. Recasting integrals for numerical computation

Here we provide steps to recast (72) into a form suitable for numerical integration.

*a. Change of variables*. We perform two successive changes of variables to recast the integrals. First, we perform the transformation $\{q,\cos\theta\}\to\{u,v\}$, where

$$u \equiv \frac{|\mathbf{k}-\mathbf{q}|}{k}, \qquad v \equiv \frac{q}{k}, \tag{A29}$$

and the inverse transformation is

$$q = vk, \qquad \cos\theta = \frac{1+v^2-u^2}{2v}. \tag{A30}$$

The determinant of the Jacobian for this transformation is,

$$\det(J_{\{q,\cos\theta\}\to\{u,v\}}) = -\partial_v q \partial_u \cos\theta = -\frac{ku}{v}. \tag{A31}$$

which implies

$$\begin{aligned}\int \mathrm{d}^3q &= \int_0^\infty q^2\mathrm{d}q\int_{-1}^1 \mathrm{d}\cos\theta\int_0^{2\pi}\mathrm{d}\phi\\ &= k^3\int_0^\infty \mathrm{d}v\, v\int_{|1-v|}^{1+v}\mathrm{d}u\, u\int_0^{2\pi}\mathrm{d}\phi.\end{aligned} \tag{A32}$$

Second, we perform $\{u,v\}\to\{s,t\}$ where

$$s \equiv u-v, \qquad t \equiv u+v-1, \tag{A33}$$

and the inverse transformation is

$$u = \frac{s+t+1}{2}, \qquad v = \frac{t-s+1}{2}. \tag{A34}$$

The determinant of the Jacobian for the second transformation is then

$$\det(J_{\{u,v\}\to\{s,t\}}) = \frac{1}{2}. \tag{A35}$$

Hence, we have[10]

$$\int_0^\infty \mathrm{d}v\int_{|1-v|}^{1+v}\mathrm{d}u = \frac{1}{2}\int_0^\infty \mathrm{d}t\int_{-1}^1 \mathrm{d}s. \tag{A36}$$

The final result is

[10]For $v<1$, the lower limit of integration over $s$ is $1-2v$. However, in this case we already have $1-2v>-1$.

$$\int \mathrm{d}^3q = \frac{k^3}{2}\int_0^\infty \mathrm{d}t \int_{-1}^{1} \mathrm{d}s\, uv \int_0^{2\pi} \mathrm{d}\phi. \tag{A37}$$

Above, we express the integrand in terms of $u$ and $v$ for convenience, though the integration itself is done in terms of $s$ and $t$.

*b. Analytic result for the $I(p,q,\tau)$ function.* We summarize the results for a radiation-dominated universe (for a more in-depth look, see e.g. [56]). At late times, we have

$$\begin{aligned} &I(vk, uk, x/k \to \infty)\\ &= \frac{1}{k^2} I(u, v, x\to\infty)\\ &\simeq \frac{1}{k^2}\frac{1}{x}\tilde{I}_A(u,v)(\tilde{I}_B(u,v)\sin x + \tilde{I}_C \cos x), \end{aligned} \tag{A38}$$

where we define

$$\tilde{I}_A(u,v) \equiv \frac{3(u^2+v^2-3)}{4u^3v^3} \tag{A39a}$$

$$\tilde{I}_B(u,v) \equiv -4uv + (u^2+v^2-3)\ln\left|\frac{3-(u+v)^2}{3-(u-v)^2}\right| \tag{A39b}$$

$$\tilde{I}_C(u,v) \equiv -\pi(u^2+v^2-3)\Theta(u+v-\sqrt{3}). \tag{A39c}$$

In the last expression, $\Theta$ is the Heaviside theta function. This result redshifts as $1/x \propto 1/a$. Using the above definitions, we compute the quantity given in (A28),

$$\begin{aligned} &\frac{Q_+(\mathbf{k},\mathbf{q})}{\cos 2\phi} I(|\mathbf{k}-\mathbf{q}|, q, \tau)\\ &= \frac{Q_\times(\mathbf{k},\mathbf{q})}{\sin 2\phi} I(|\mathbf{k}-\mathbf{q}|, q, \tau)\\ &= \frac{v^2k^2}{\sqrt{2}}\frac{4v^2-(1+v^2-u^2)^2}{4v^2} I(uk, vk, x/k)\\ &\equiv \frac{\tilde{\mathcal{J}}(u,v)}{\sqrt{2}} k^2 I(uk, vk, x/k), \end{aligned} \tag{A40}$$

where we have used dimensionless conformal time $x = k\tau$ and defined

$$\tilde{\mathcal{J}}(u,v) = \frac{4v^2-(1+v^2-u^2)^2}{4}. \tag{A41}$$

When computing the GW power spectrum we are generically interested in the time-averaged quantity

$$\begin{aligned} &\overline{k^2 I(v_1k, u_1k, x/k\to\infty) k^2 I(v_2k, u_2k, x/k\to\infty)}\\ &= \frac{1}{2x^2}\tilde{I}_A(u_1,v_1)\tilde{I}_A(u_2,v_2)\\ &\quad\times[\tilde{I}_B(u_1,v_1)\tilde{I}_B(u_2,v_2) + \tilde{I}_C(u_1,v_1)\tilde{I}_C(u_2,v_2)]. \end{aligned} \tag{A42}$$

*c. Azimuthal angle integration.* In the disconnected contribution (72), the only $\phi$-dependent factors in the integrands are $\sin 2\phi$ and $\cos 2\phi$, coming from $Q_\lambda$ factors. For each polarization, we then have

$$\int_0^{2\pi}\mathrm{d}\phi \sin^2(2\phi) = \int_0^{2\pi}\mathrm{d}\phi\cos^2(2\phi) = \pi. \tag{A43}$$

Finally, we are ready to numerically compute the GW energy density (75) which is defined in terms of the dimensionless polarization-averaged GW power spectrum

$$\sum_\lambda \Delta_\lambda^2(\tau,k) = \frac{k^3}{2\pi^2}\sum_\lambda P_\lambda(\tau,k). \tag{A44}$$

Using our recasted variables, the result is

$$\begin{aligned} \Omega_{\mathrm{GW}}(k)|_{\mathrm{d}} = &\frac{2}{48\alpha^2}\left(\frac{k^3}{2\pi^2}\right)^2\\ &\times\int_0^\infty \mathrm{d}t\int_{-1}^1 \mathrm{d}s\, uv\tilde{\mathcal{J}}(u,v)^2\tilde{I}_A(u,v)^2[\tilde{I}_B(u,v)^2\\ &+\tilde{I}_C(u,v)^2]P_\zeta(uk)P_\zeta(vk) \end{aligned} \tag{A45}$$

More compactly,

$$\Omega_{\mathrm{GW}}(k)|_{\mathrm{d}} = \frac{2}{48\alpha^2}\int_0^\infty \mathrm{d}t\int_{-1}^1 \mathrm{d}s\,\mathcal{K}_{\mathrm{d}}(u,v)\Delta_\zeta^2(uk)\Delta_\zeta^2(vk) \tag{A46}$$

where we define the following the Kernel functions $\mathcal{K}_{\mathrm{d}}$ for simplified notation,

$$\mathcal{K}_{\mathrm{d}}(u,v) = (uv)^{-2}\tilde{\mathcal{J}}(u,v)^2\tilde{I}_A(u,v)^2[\tilde{I}_B(u,v)^2 + \tilde{I}_C(u,v)^2]. \tag{A47}$$

### 5. Useful formula

The projection operator $Q_\lambda$ (65) is defined as,

$$Q_\lambda(\mathbf{k},\mathbf{q}) \equiv \epsilon_\lambda^{ij}(\mathbf{k})q_iq_j = -\epsilon_\lambda^{ij}(\mathbf{k})(\mathbf{k}-\mathbf{q})_iq_j, \tag{A48}$$

where the second equality follows from $\epsilon_\lambda^{ij}(\mathbf{k})k_i = 0$. If we explicitly set $\hat{k} = \hat{z}$, we have $\mathbf{q} = q(\sin\theta\cos\phi, \sin\theta\sin\phi, \cos\theta)$, where $\theta$ and $\phi$ are polar and azimuthal angles. This leads to the expressions,

$$Q_+(\mathbf{k},\mathbf{q}) = \frac{q^2}{\sqrt{2}}\sin^2\theta\cos(2\phi),$$
$$Q_\times(\mathbf{k},\mathbf{q}) = \frac{q^2}{\sqrt{2}}\sin^2\theta\sin(2\phi). \tag{A49}$$

Since $\epsilon_\lambda(\mathbf{k})$ is orthogonal to $\mathbf{k}$ we have

$$Q_\lambda(\mathbf{k},\mathbf{q}) = Q_\lambda(\mathbf{k},\mathbf{q}+c\mathbf{k}), \tag{A50}$$

for any constant $c$. $Q_\lambda(\mathbf{k},\mathbf{q})$ is also symmetric under $\mathbf{k}\to-\mathbf{k}$ and $\mathbf{q}\to-\mathbf{q}$:

$$Q_\lambda(\mathbf{k},\mathbf{q}) = Q_\lambda(-\mathbf{k},\mathbf{q}) = Q_\lambda(\mathbf{k},-\mathbf{q}) = Q_\lambda(-\mathbf{k},-\mathbf{q}). \tag{A51}$$

Using (71) we see that

$$f(p,q,\tau) = f(q,p,\tau) \tag{A52}$$

and so

$$I(p,q,\tau) = I(q,p,\tau). \tag{A53}$$

*a. Bessel functions*. The following formulas are helpful for computations involving Bessel functions:

$$J_{1/2}(x) = \sqrt{\frac{2}{\pi x}}\sin x,$$
$$Y_{1/2}(x) = -\sqrt{\frac{2}{\pi x}}\cos x,$$
$$J_{3/2}(x) = \sqrt{\frac{2}{\pi x}}\left(\frac{\sin x}{x} - \cos x\right),$$
$$Y_{3/2}(x) = -\sqrt{\frac{2}{\pi x}}\left(\frac{\cos x}{x} - \sin x\right). \tag{A54}$$


[1] D. Baumann, Inflation, in *Theoretical Advanced Study Institute in Elementary Particle Physics: Physics of the Large and the Small* (World Scientific, 2011), pp. 523–686, 10.1142/9789814327183_0010.

[2] Y. Akrami *et al.* (Planck Collaboration), Planck 2018 results. X. Constraints on inflation, Astron. Astrophys. **641**, A10 (2020).

[3] K. K. Boddy *et al.*, Snowmass2021 theory frontier white paper: Astrophysical and cosmological probes of dark matter, J. High Energy Astrophys. **35**, 112 (2022).

[4] G. Domènech, Scalar induced gravitational waves review, Universe **7**, 398 (2021).

[5] A. M. Green and B. J. Kavanagh, Primordial black holes as a dark matter candidate, J. Phys. G **48**, 043001 (2021).

[6] B. Carr and F. Kuhnel, Primordial black holes as dark matter: Recent developments, Annu. Rev. Nucl. Part. Sci. **70**, 355 (2020).

[7] P. Ivanov, P. Naselsky, and I. Novikov, Inflation and primordial black holes as dark matter, Phys. Rev. D **50**, 7173 (1994).

[8] J. Garcia-Bellido and E. Ruiz Morales, Primordial black holes from single field models of inflation, Phys. Dark Universe **18**, 47 (2017).

[9] G. Ballesteros and M. Taoso, Primordial black hole dark matter from single field inflation, Phys. Rev. D **97**, 023501 (2018).

[10] N. C. Tsamis and R. P. Woodard, Improved estimates of cosmological perturbations, Phys. Rev. D **69**, 084005 (2004).

[11] W. H. Kinney, Horizon crossing and inflation with large eta, Phys. Rev. D **72**, 023515 (2005).

[12] S. Hooshangi, A. Talebian, M. H. Namjoo, and H. Firouzjahi, Multiple field ultraslow-roll inflation: Primordial black holes from straight bulk and distorted boundary, Phys. Rev. D **105**, 083525 (2022).

[13] S. Kasuya and M. Kawasaki, Axion isocurvature fluctuations with extremely blue spectrum, Phys. Rev. D **80**, 023516 (2009).

[14] M. Kawasaki, N. Kitajima, and T. T. Yanagida, Primordial black hole formation from an axionlike curvaton model, Phys. Rev. D **87**, 063519 (2013).

[15] D. J. H. Chung and H. Yoo, Elementary theorems regarding blue isocurvature perturbations, Phys. Rev. D **91**, 083530 (2015).

[16] D. J. H. Chung and A. Upadhye, Search for strongly blue axion isocurvature, Phys. Rev. D **98**, 023525 (2018).

[17] D. J. H. Chung and S. C. Tadepalli, Analytic treatment of underdamped axionic blue isocurvature perturbations, Phys. Rev. D **105**, 123511 (2022).

[18] A. Talebian, A. Nassiri-Rad, and H. Firouzjahi, Stochastic effects in axion inflation and primordial black hole formation, Phys. Rev. D **105**, 103516 (2022).

[19] P. W. Graham, J. Mardon, and S. Rajendran, Vector dark matter from inflationary fluctuations, Phys. Rev. D **93**, 103520 (2016).

[20] A. L. Erickcek and K. Sigurdson, Reheating effects in the matter power spectrum and implications for substructure, Phys. Rev. D **84**, 083503 (2011).

[21] J. Barir, M. Geller, C. Sun, and T. Volansky, Gravitational waves from incomplete inflationary phase transitions, arXiv:2203.00693.

[22] D. J. H. Chung, E. W. Kolb, A. Riotto, and L. Senatore, Isocurvature constraints on gravitationally produced superheavy dark matter, Phys. Rev. D **72**, 023511 (2005).

[23] A. A. Starobinsky, Stochastic de sitter (inflationary) stage in the early universe, in *Field Theory, Quantum Gravity and Strings. Lecture Notes in Physics*, edited by H. J. de Vega and N. Sánchez, Vol. 246 (Springer, Berlin, Heidelberg, 1988).

[24] A. A. Starobinsky and J. Yokoyama, Equilibrium state of a selfinteracting scalar field in the de Sitter background, Phys. Rev. D **50**, 6357 (1994).

[25] A. D. Linde and V. F. Mukhanov, Nongaussian isocurvature perturbations from inflation, Phys. Rev. D **56**, R535 (1997).

[26] K. Enqvist and M. S. Sloth, Adiabatic CMB perturbations in pre-big bang string cosmology, Nucl. Phys. **B626**, 395 (2002).

[27] T. Moroi and T. Takahashi, Effects of cosmological moduli fields on cosmic microwave background, Phys. Lett. B **522**, 215 (2001).

[28] D. H. Lyth and D. Wands, Generating the curvature perturbation without an inflaton, Phys. Lett. B **524**, 5 (2002).

[29] E. W. Kolb and M. S. Turner, *The Early Universe* (CRC Press, Boca Raton, 1990), Vol. 69, 10.1201/9780429492860.

[30] K. A. Malik and D. Wands, Cosmological perturbations, Phys. Rep. **475**, 1 (2009).

[31] D. Wands, K. A. Malik, D. H. Lyth, and A. R. Liddle, A new approach to the evolution of cosmological perturbations on large scales, Phys. Rev. D **62**, 043527 (2000).

[32] M. Sasaki, Y. Nambu, and K.-i. Nakao, Classical behavior of a scalar field in the inflationary universe, Nucl. Phys. **B308**, 868 (1988).

[33] Y. Nambu and M. Sasaki, Stochastic stage of an inflationary universe model, Phys. Lett. B **205**, 441 (1988).

[34] P. W. Graham and A. Scherlis, Stochastic axion scenario, Phys. Rev. D **98**, 035017 (2018).

[35] T. Markkanen, A. Rajantie, S. Stopyra, and T. Tenkanen, Scalar correlation functions in de Sitter space from the stochastic spectral expansion, J. Cosmol. Astropart. Phys. 08 (2019) 001.

[36] A. R. Liddle and S. M. Leach, How long before the end of inflation were observable perturbations produced?, Phys. Rev. D **68**, 103503 (2003).

[37] S. Dodelson and L. Hui, A horizon ratio bound for inflationary fluctuations, Phys. Rev. Lett. **91**, 131301 (2003).

[38] L. F. Abbott, E. Farhi, and M. B. Wise, Particle production in the new inflationary cosmology, Phys. Lett. **117B**, 29 (1982).

[39] A. D. Dolgov and A. D. Linde, Baryon asymmetry in inflationary universe, Phys. Lett. B **116B**, 329 (1982).

[40] A. Albrecht, P. J. Steinhardt, M. S. Turner, and F. Wilczek, Reheating an inflationary universe, Phys. Rev. Lett. **48**, 1437 (1982).

[41] D. I. Podolsky, G. N. Felder, L. Kofman, and M. Peloso, Equation of state and beginning of thermalization after preheating, Phys. Rev. D **73**, 023501 (2006).

[42] J. B. Munoz and M. Kamionkowski, Equation-of-state parameter for reheating, Phys. Rev. D **91**, 043521 (2015).

[43] L. Dai, M. Kamionkowski, and J. Wang, Reheating constraints to inflationary models, Phys. Rev. Lett. **113**, 041302 (2014).

[44] K. D. Lozanov and M. A. Amin, Equation of state and duration to radiation domination after inflation, Phys. Rev. Lett. **119**, 061301 (2017).

[45] D. Maity and P. Saha, (P)reheating after minimal Plateau inflation and constraints from CMB, J. Cosmol. Astropart. Phys. 07 (2019) 018.

[46] S. Antusch, D. G. Figueroa, K. Marschall, and F. Torrenti, Energy distribution and equation of state of the early Universe: Matching the end of inflation and the onset of radiation domination, Phys. Lett. B **811**, 135888 (2020).

[47] R. Allahverdi, R. Brandenberger, F.-Y. Cyr-Racine, and A. Mazumdar, Reheating in inflationary cosmology: Theory and applications, Annu. Rev. Nucl. Part. Sci. **60**, 27 (2010).

[48] J. Chluba, R. Khatri, and R. A. Sunyaev, CMB at $2 \times 2$ order: The dissipation of primordial acoustic waves and the observable part of the associated energy release, Mon. Not. R. Astron. Soc. **425**, 1129 (2012).

[49] J. Chluba *et al.*, Spectral distortions of the CMB as a probe of inflation, recombination, structure formation and particle physics: Astro2020 science white paper, Bull. Am. Astron. Soc. **51**, 184 (2019).

[50] V. S. H. Lee, A. Mitridate, T. Trickle, and K. M. Zurek, Probing small-scale power spectra with pulsar timing arrays, J. High Energy Phys. 06 (2021) 028.

[51] K. Van Tilburg, A.-M. Taki, and N. Weiner, Halometry from astrometry, J. Cosmol. Astropart. Phys. 07 (2018) 041.

[52] D. J. Fixsen and J. C. Mather, The spectral results of the far-infrared absolute spectrophotometer instrument on COBE, Astrophys. J. **581**, 817 (2002).

[53] A. Riotto, The primordial black hole formation from single-field inflation is not ruled out, arXiv:2301.00599.

[54] K. N. Ananda, C. Clarkson, and D. Wands, The cosmological gravitational wave background from primordial density perturbations, Phys. Rev. D **75**, 123518 (2007).

[55] D. Baumann, P. J. Steinhardt, K. Takahashi, and K. Ichiki, Gravitational wave spectrum induced by primordial scalar perturbations, Phys. Rev. D **76**, 084019 (2007).

[56] K. Kohri and T. Terada, Semianalytic calculation of gravitational wave spectrum nonlinearly induced from primordial curvature perturbations, Phys. Rev. D **97**, 123532 (2018).

[57] J. R. Espinosa, D. Racco, and A. Riotto, A cosmological signature of the SM Higgs instability: Gravitational waves, J. Cosmol. Astropart. Phys. 09 (2018) 012.

[58] P. Adshead, K. D. Lozanov, and Z. J. Weiner, Non-Gaussianity and the induced gravitational wave background, J. Cosmol. Astropart. Phys. 10 (2021) 080.

[59] J.-P. Li, S. Wang, Z.-C. Zhao, and K. Kohri, Primordial non-Gaussianity and anisotropies in gravitational waves induced by scalar perturbations, arXiv:2305.19950.

[60] Z.-C. Chen, C. Yuan, and Q.-G. Huang, Pulsar timing array constraints on primordial black holes with NANOGrav 11-year dataset, Phys. Rev. Lett. **124**, 251101 (2020).

[61] S. Garcia-Saenz, L. Pinol, S. Renaux-Petel, and D. Werth, No-go theorem for scalar-trispectrum-induced gravitational waves, J. Cosmol. Astropart. Phys. 03 (2023) 057.

[62] C. Unal, Imprints of primordial non-Gaussianity on gravitational wave spectrum, Phys. Rev. D **99**, 041301 (2019).

[63] V. Atal and G. Domènech, Probing non-Gaussianities with the high frequency tail of induced gravitational waves, J. Cosmol. Astropart. Phys. 06 (2021) 001.

[64] M. Maggiore, Gravitational wave experiments and early universe cosmology, Phys. Rep. **331**, 283 (2000).

[65] K. Schmitz, New sensitivity curves for gravitational-wave signals from cosmological phase transitions, J. High Energy Phys. 01 (2021) 097.

[66] A. Sesana *et al.*, Unveiling the gravitational universe at $\mu$-Hz frequencies, Exp. Astron. **51**, 1333 (2021).

[67] M. Braglia and S. Kuroyanagi, Probing prerecombination physics by the cross-correlation of stochastic gravitational waves and CMB anisotropies, Phys. Rev. D **104**, 123547 (2021).

[68] G. Agazie *et al.* (NANOGrav Collaboration), The NANOGrav 15 yr data set: Evidence for a gravitational-wave background, Astrophys. J. Lett. **951**, L8 (2023).

[69] J. Antoniadis *et al.* (EPTA Collaboration), The second data release from the European pulsar timing array III. Search for gravitational wave signals, arXiv:2306.16214.

[70] J. Antoniadis *et al.* (EPTA Collaboration), The second data release from the European pulsar timing array - I. The dataset and timing analysis, Astron. Astrophys. **678**, A48 (2023).

[71] D. J. Reardon *et al.*, Search for an isotropic gravitational-wave background with the Parkes pulsar timing array, Astrophys. J. Lett. **951**, L6 (2023).

[72] H. Xu *et al.*, Searching for the nano-hertz stochastic gravitational wave background with the Chinese pulsar timing array data release I, Res. Astron. Astrophys. **23**, 075024 (2023).

[73] A. Afzal *et al.* (NANOGrav Collaboration), The NANOGrav 15 yr data set: Search for signals from new physics, Astrophys. J. Lett. **951**, L11 (2023).

[74] J. Antoniadis *et al.* (EPTA Collaboration), The second data release from the European pulsar timing array: V. Implications for massive black holes, dark matter and the early Universe, arXiv:2306.16227.